Solid Earth Discuss., https://doi.org/10.5194/se-2018-136
Manuscript under review for journal Solid Earth
Discussion started: 3 January 2019
© Author(s) 2019. CC BY 4.0 License.

# Fault-controlled dolomitization in the Montagna dei Fiori Anticline (Central Apennines, Italy): Record of a dominantly pre-orogenic fluid migration

Mahtab Mozafari[1], Rudy Swennen[2], Fabrizio Balsamo[1], Hamdy El Desouky[2,3], Fabrizio Storti[1] and Conxita Taberner[4]

*1- NEXT - Natural and Experimental Tectonics Research Group - Department of Chemistry, Life Sciences and Environmental Sustainability, University of Parma, Italy.*
*2- Department of Earth and Environmental Sciences, KU Leuven, Belgium.*
*3- Geology Department, Faculty of Science, Menoufia University, Menoufia, Egypt*
*4- Shell Global Solutions International B.V., Amsterdam, The Netherlands*
Correspondence: Mahtab Mozafari (mahtab_mozafari@yahoo.com) and Fabrizio Storti (Fabrizio.Storti@unipr.it)

## Abstract

The Lower Jurassic platform and basinal deposits exposed in the Montagna dei Fiori Anticline (Central Apennines, Italy) are pervasively affected by dolomitization. Based on the integration of field work, petrography, and geochemistry, two fault-related dolomitization events were recognized and interpreted as occurred before and during the Apenninic orogeny, respectively. Fluid inclusion analysis indicates moderate to elevated salinity values of 3.5 to 20.5 and 12.8 to 18.6 eq. wt. % NaCl, in the first and the second event, respectively. The estimated salinities, in combination with $\delta^{18}O$ values and $^{87}Sr/^{86}Sr$ ratios, suggest significant involvement of evaporitic fluids in both events, most likely derived from the underlying Upper Triassic Burano Formation. In addition, the $^{87}Sr/^{86}Sr$ ratios up to 0.70963 suggest the circulation of deep-sourced fluids that interacted with siliciclastics and/or the crystalline basement during the dolomitization events. The first dolomitization event which is also considered as the most pervasive one started prior to the significant burial conditions, as reflected in homogenization temperatures of their fluid inclusions being mostly below about 40-50°C. Two major dolomite types (D1 and D2) were recognized as pertaining to this event, both postdated by high amplitude bed-parallel stylolites. This relationship supports a syn-burial, pre layer-parallel shortening dolomitization, interpreted as controlled by the extensional fault pattern affecting the carbonate succession before its involvement in the Apenninic thrust wedge. A possible geodynamic

Solid Earth Discuss., https://doi.org/10.5194/se-2018-136
Manuscript under review for journal Solid Earth
Discussion started: 3 January 2019
© Author(s) 2019. CC BY 4.0 License.

framework for this dolomitization event is Early to Late Jurassic rift-related extensional tectonism.

The second dolomitization event initiated with a dolomite type (D3) characterized by a slight temperature upturn (up to 73°C), followed by a second type (D4) with markedly higher homogenization temperatures (up to 105°C), interpreted as associated with the inflow of hydrothermal fluids, possibly related to major changes in the permeability architecture of faults during early- to syn-thrusting and folding activity. Eventually, D4 was overprinted by a late generation of dolomite veins (D5) interpreted as associated with late orogenic extensional faulting in the backlimb of the Montagna dei Fiori Anticline. Based on the timing of deformation in the Montagna dei Fiori Anticline, D3 to D5 dolomitization likely occurred in Late Miocene to Pliocene times. The findings regarding characteristics and timing of dolomitization here illustrates the long-term controlling role of the eveporitic detachments in dolomitization process. Our data shows the Mg-rich fluids most likely derived from these evaporites may prime the tectonically involved successions for repeated dolomitization, and formation of potential reservoirs in sequential tectonic modifications (extensional vs. compressional).

## 1 Introduction

Fault-controlled dolomitization has been the focus of attention in many studies during the last decades due to its influential role in modifying the petrophysical properties of rocks and, hence, anisotropy in fluid migration pathways, and, ultimately on reservoir quality (e.g. Purser et al., 1994; Montanez, 1994; Zempolich and Hardie, 1997; Vandeginste et al., 2005; Davies and Smith, 2006; Sharp et al. 2010). The mechanical and hydrological behaviour of fault zones are in turn influenced by fluid-rock interactions and diagenetic modifications (e.g. Gale et al., 2004; Laubach et al., 2010; Clemenzi et al., 2015). It follows that the mutual interplay between fault activity and fluid-driven rock-fluid interaction can trigger dolomitization of carbonates and, consequently, variations in physico-chemical properties of fluids through time and space. Leaking or sealing behaviours of fault zones during deformation are key controls for fault-related fluid circulation. A detailed understanding of such an interplay is thus necessary to improve our capability of making reliable predictions of fault-related dolomitization in carbonate reservoirs. Studying outcrop analogues provides fundamental support to meet this requirement (e.g. Swennen et al., 2012; Dewit et al., 2014; Bistacchi et al., 2015).

Solid Earth Discuss., https://doi.org/10.5194/se-2018-136
Manuscript under review for journal Solid Earth
Discussion started: 3 January 2019
© Author(s) 2019. CC BY 4.0 License.



The Lower Jurassic to Lower Cretaceous Umbria-Marche passive margin carbonate succession, in the Central Apennines (Italy), is intensely affected by localized dolomitization both in the onshore fold-and-thrust belt and in offshore foredeep and foreland areas (e.g. Murgia et al., 2004; Pierantoni et al., 2013). The dolomitized intervals are well-exposed in the core of the Montagna dei Fiori Anticline (e.g. Ronchi et al., 2003), where the dolomitized Lower Jurassic intervals (Calcare Massiccio, Bugarone and Corniola Formations) and their relationships with fault zones allow to study the mutual influence between deformation structures and dolomitized intervals (Fig. 1). These intervals, known as the Castel Manfrino Dolostones (Crescenti, 1969; Mattei, 1987; Koopman, 1983), have been previously studied by Ronchi et al. (2003) at its reference section, the Castel Manfrino location, in the central sector of the Montagna dei Fiori Anticline (Fig. 2). A fault-controlled dolomitization model and the relative timing of dolomitization were proposed by Ronchi (2003). Recent re-evaluation of dolostone distribution in the Montagna dei Fiori Anticline (Storti et al., 2017a), showed that the dimension of the dolomitized geobodies (Fig. 2) is much more significant than what was previously mapped by Mattei (1987). Dolostones are distributed within fault damage zones and in the laterally adjacent carbonate rocks, and in intersection areas between fault sets, for a total area in map view of more than 1.5 $km^2$ (Storti et al., 2017a).

The structural pattern of the Montagna dei Fiori Anticline documents the overprinting of extensional and contractional deformation along major fault zones. Although challenging, the preserved structural framework in this anticline provides an opportunity to study the direct but complex regional tectonic controls on dolomitization in carbonate successions undergoing multiple deformation events, from rifting to folding and thrusting. This contribution integrates field mapping, new petrographic, geochemical, and microthermometric analyses, with structural studies to characterize the temporal record of fault-controlled diagenetic phases and, more specifically, dolomitization in the carbonatic succession outcropping in the Montagna dei Fiori Anticline. Therefore provides insights into the structural controls on regional fluid flow and their chemical evolution through time. These findings might be of relevance for exploration and reservoir quality prediction onshore and offshore the Apennines and Southern Alps. Moreover, this work provides additional evidence of the potential influence of fluids derived from evaporitic detachment levels in modifications of geochemical trends and petrophysical properties of the overlying carbonate rocks.

Solid Earth Discuss., https://doi.org/10.5194/se-2018-136
Manuscript under review for journal Solid Earth
Discussion started: 3 January 2019
© Author(s) 2019. CC BY 4.0 License.



## 2 Geological setting

The Montagna dei Fiori Anticline is a NNW-SSE striking, thrust-related fold located at the mountain front of the Central Apennines (Fig. 1). The geodynamic evolution of the Apennines is generally known to be the result of the superposition of NE-SW compression (in present-day geographic coordinates), related to the convergence between Eurasia and Africa plates since Late Cretaceous times (Elter et al., 1975; Dewey et al., 1989; Patacca et al., 1992), on a rifting-related tectono-sedimentary architecture produced by Early Jurassic extension (e.g., Centamore et al., 1971). In such a framework, the Central Apennines developed during Miocene to Plio-Pleistocene times (e.g. Parotto and Praturlon, 1975; Barchi et al., 1998; Mazzoli et al., 2002; Bollati et al., 2012).

The Central Apennines involves the Umbria-Marche succession, which essentially includes Triassic to Miocene carbonates and marls, covered by Miocene to Pliocene syn-orogenic clastic sediments (Fig. 1). The pre-orogenic succession, from bottom to top, includes Late Triassic evaporites, dolomites and limestones (Burano Formation), Early to Late Jurassic platform and basinal limestones and dolostones (Calcare Massiccio, Corniola, Rosso Ammonitico, Calcari a Posidonia and Calcari ad Aptici Formations), and Cretaceous to Early Miocene basinal carbonates (Maiolica, Marne a Fucoidi, Scaglia and Biscaro Formations). In general, the lower part of Burano Formation is overlaid by the fluvio-deltaic siliciclastics of the Verrucano Formation (Middle-Late Triassic) (Tongiorgi et al., 1977; Ghisetti and Vezzani, 2000; Tavani et al., 2008). Nevertheless, the existence of these siliciclastics in the Montagna dei Fiori area is not yet proved. Syn-orogenic deposits include Miocene marls and turbiditic sandstones (Marne con Cerrogna and Laga Formations) (Artoni, 2013 and references therein).

The deposition of the Calcare Massiccio Formation, dated as Hettangian-Sinemurian and with a total thickness varying between 300 to 700 m (Pialli, 1971), records an important extension pulse in the evolution of Tethyan rifting. The following facies are observed in the lower part of the Calcare Massiccio Formation: oncoid-rich peloidal pack- to grainstones in alternation with peloidal wacke- to packstones including horizons of algal bindstones (Calcare Massiccio A; Brandano et al., 2016). The upper part is made up of beds of skeletal and coated grain wacke- to grainstones including microoncoids, echinoderms, calcareous and siliceous sponges, bivalves, gastropods and ammonites (Calcare Massiccio B; Brandano et al., 2016). The lower part has been interpreted as having been deposited in a peritidal environment, while the

Solid Earth Discuss., https://doi.org/10.5194/se-2018-136
Manuscript under review for journal Solid Earth
Discussion started: 3 January 2019
© Author(s) 2019. CC BY 4.0 License.



upper part corresponds to lower to middle shelf depositional environments, characterized by a general deepening upward trend associated with extensional faulting and drowning of the platform, coupled with subsidence and deposition of the overlying Corniola Formation in the pelagic areas (Sinemurian-Toarcian; Colacicchi et al., 1975; Morettini et al., 2002; Bosence et al., 2009; Marino and Santantonio, 2010; Brandano et al., 2016). Overall, the Early Jurassic rifting led to the growth of the Calcare Massiccio Formation in a carbonate platform setting, followed by faulting and drowning, and development of pelagic intrabasins filled by syn-rift sediments (Fig. 1c; Bernoulli et al. 1979; Santantonio and Carminati, 2011). Condensed pelagic limestones of the Bugarone Formation (Lower Pliensbachian-Lower Tithonian; Bugarone Group in Pierantoni et al., 2013) occur at the top of the Calcare Massiccio Formation where it formed fault-controlled highs marking the regional drowning of the carbonate platform (Santantonio and Carminati, 2011). In the Montagna dei Fiori, the geologic framework of the outcropping Calcare Massiccio Formation is still a matter of debate between a fault-related tectonosedimentary pattern (Mattei, 1987; Storti et al., 2017b), and a gravity-driven, olistolith hypothesis (Di Francesco et al, 2010; Santantonio et al., 2017). However, recent detailed work in the Salinello valley (Storti et al., 2017a; 2018) documented that major outcrops of Calcare Massiccio are bounded by mostly ~ E-W and ~ N-S striking fault zones showing extensional kinematics and dominantly affecting the Jurassic rocks older than the Maiolica Formation (Fig. 2A, e.g. sites 1 to 4). Overprinting relations indicate that ~ E-W deformation structures are systematically younger than the ~ N-S ones. Similar trends were observed in syn-rift fault zones in other anticlines of the Central Apennines (e.g. Cooper and Burbi, 1986; Alvarez, 1989; Chilovi et al., 2002).

Such a tectonosedimentary inheritance was involved in the growth of the Montagna dei Fiori Anticline, which initiated during the Late Miocene (Mazzoli et al., 2002; Artoni, 2003) and progressively evolved into the upper thrust sheet of a well-developed antiformal stack until Plio-Pleistocene times (e.g. Ghisetti et al., 1993; Calamita et al., 1994; Artoni, 2013). A major structural feature trending parallel to the Montagna dei Fiori Anticline and dissecting it is the Montagna dei Fiori Fault, a NNW-SSE striking extensional fault system cutting at high angle through the folded footwall rocks, typically at the forelimb-crest transition (Figs. 1, 2). This fault system juxtaposes intensely deformed Late Miocene sediments in the hanging wall, against dolomitized and undolomitized Lower Jurassic and Cretaceous limestones in the footwall (Figs.

Solid Earth Discuss., https://doi.org/10.5194/se-2018-136
Manuscript under review for journal Solid Earth
Discussion started: 3 January 2019
© Author(s) 2019. CC BY 4.0 License.



1 and 2). The development of the Montagna dei Fiori Fault has been alternatively interpreted as either a pre- (e.g. Calamita et al., 1994, Mazzoli, 2002; Scisciani et al., 2002) or late-folding (Ghisetti and Vezzani, 2000) feature. More recently, the origin of the Montagna dei Fiori Fault has been ascribed to the mutual interaction between horizontal shortening and uplift, and episodic gravitational re-equilibration during antiformal stacking underneath the anticline during Plio-Pleistocene times (Storti et al., 2018).

## 3 Methodology

The stratigraphic and deformational features of dolostones were analyzed in more than 60 outcrops. The distribution of dolomitized intervals as well as their cross-cutting relationships with bedding planes, stylolites, veins and structures were ground-truthed and sampled. For petrographic analyses, 130 polished thin sections were studied with standard petrographic methods (transmitted and UV-fluorescent light microscopy). Dolomite crystal morphology and texture is based on the classification proposed by Sibley and Gregg (1987).

The rock slabs and thin sections were stained using Alizarine Red S and potassium ferricyanide (Dickson, 1966) to discriminate dolomite from calcite and evaluate their iron content. Cold cathodoluminescence microscopy (CL) was carried out on representative thin sections (n = 80) at KU Leuven University (Belgium) using a Technosyn cathodoluminescence device (8-15 kV, 200-400 μA gun current, 0.05 Torr vacuum and 5 mm beam width).

$\delta^{13}C$ and $\delta^{18}O$ analysis were carried out on 117 samples. Powder samples (150 - 200 μg) were obtained by applying a New Wave Research micromilling device and a dental drill at KU Leuven University (Belgium). The analysis was conducted at Parma University (Italy) and the Friedrich-Alexander-Universität (Erlangen-Nürnberg, Germany) laboratories using Finnigan DeltaPlus V and ThermoFinnigan 252 mass spectrometers, respectively. The carbonate powders were reacted with 100% phosphoric acid at constant temperature of 75°C. Several additional $CO_2$ reference gases (NBS18, NBS19, MAB99, and a pure Carrara marble) with known isotopic ratio were analyzed during the measurements to determine the $\delta^{13}C$ and $\delta^{18}O$ values of the sample. Reproducibility was checked by replicate analysis of laboratory standards and was better than ±0.1‰ for $\delta^{13}C$ and ±0.2‰ for $\delta^{18}O$ at Parma University and ±0.04 for $\delta^{13}C$ and ±0.05‰ for $\delta^{18}O$ at Friedrich-Alexander-Universität. Oxygen isotope composition of dolomites was corrected using the acid fractionation factors given by Rosenbaum and Sheppard (1986). Duplicate homogeneous samples measured in both labs for inter-laboratory reproducibility show

Solid Earth Discuss., https://doi.org/10.5194/se-2018-136
Manuscript under review for journal Solid Earth
Discussion started: 3 January 2019
© Author(s) 2019. CC BY 4.0 License.



186 $\delta^{13}C$ and $\delta^{18}O$ values within the acceptable range of error deviation (±0.1‰) both for $\delta^{13}C$ and
187 $\delta^{18}O$. All carbon and oxygen values are reported in per mil, relative to the "Vienna PDB scale"
188 (V-PDB).

189 A total number of 21 samples were analyzed for their $^{87}Sr/^{86}Sr$ ratios. The analyses were
190 conducted at the Department of Analytical Chemistry, Ghent University (Belgium) and at the
191 Vrije Universiteit Amsterdam (the Netherlands). NIST SRM 987 was used as the international Sr
192 standard in both labs. At Ghent University, 15 sample powders (20 mg) were collected using a
193 dental drill device. The $^{87}Sr/^{86}Sr$ ratio measurements were performed using a Thermo Scientific
194 Neptune Multi-collector Inductively Coupled Plasma Mass Spectrometer (MC-ICP-MS)
195 instrument. Within the external precision, repeated analyses of the international Sr standard
196 yielded an average $^{87}Sr/^{86}Sr$ ratio of 0.710271 ± 0.000023 (2SD, n = 43), in agreement with the
197 accepted $^{87}Sr/^{86}Sr$ ratio of 0.710248 for this reference sample (Thirlwall, 1991). At Vrije
198 Universiteit Amsterdam, 6 sample powders (2 - 3 mg) were collected using a New Wave
199 Research micromilling device. Analyses were performed using a ThermoElectron Triton plus
200 TIMS instrument. In order to monitor and document the system's performance, repeated analyses
201 of the international Sr standard (n = 58) were carried out on load sizes of 10 ng and 100 ng which
202 yielded average $^{87}Sr/^{86}Sr$ ratios of 0.710245±0.000022 (2SD) and 0.710242±0.000008 (2SD),
203 respectively. In both labs mass discrimination correction was performed via internal
204 normalization using Russell's exponential law and the accepted value (0.1194; Steiger and Jager,
205 1977) of the invariant $^{86}Sr/^{88}Sr$ ratio.

206 Fluid inclusion microthermometry analysis was performed on 11 doubly polished wafers
207 (80-130 μm in thickness). Measurements were carried out at Parma University (Italy) using
208 Linkam THMSG-600 and Linkam MDS-600 heating-cooling stages coupled with a Leica DM
209 2500 microscope. The stages were calibrated by synthetic Syn Flinc™ fluid inclusion standards.
210 A 100x objective was used during the microthermometry runs of the small inclusions. The
211 microthermometry data were collected following the Fluid Inclusion Assemblage (FIA) approach
212 described in Goldstein and Reynolds (1994) for carbonate minerals. The salinities are reported in
213 equivalent weight percent NaCl (eq. wt. % NaCl) and were calculated based on the equation of
214 Bodnar (1993).

215 In order to perform a high resolution petrography, Scanning Electron Microscope (SEM)
216 and Back-scattered Scanning Electron Microscope (BSEM) analyses were conducted using a

Solid Earth Discuss., https://doi.org/10.5194/se-2018-136
Manuscript under review for journal Solid Earth
Discussion started: 3 January 2019
© Author(s) 2019. CC BY 4.0 License.



Jeol 6400 Scanning Electron Microscope (SEM) equipped with an Oxford EDS (Energy Dispersive System). Operating conditions were 15 kV and 1.2 nA, electron beam about 1 μm in diameter and 100 s counting time; errors are ±2-5% for major elements and ±5-10% for minor components. The analysis focused mainly on detecting possible dolomite crystals inside the bed perpendicular stylolites affecting the Cretaceous Scaglia Formation.

## 4 Results

### 4.1 Field observation and distribution of the dolomitized bodies

Dolomitization affected the Calcare Massiccio, Bugarone and Corniola Formations. There is no evidences of dolomitization in the overlying and immediate surrounding successions (e.g. Maiolica and Scaglia Formations), though the base of Maiolica Formation is reported as dolomitized in the Central Apennines onshore (e.g. Pierantoni et al., 2013) and offshore areas (Murgia et al., 2004). Dolomitized intervals are folded in the forelimb of the Montagna dei Fiori Anticline and are abruptly truncated by the Montagna dei Fiori Fault, which juxtaposes them against intensely foliated Scaglia, Bisciaro and Marne con Cerrogna Formations (Figs. 2 and 3). The distribution of dolomitized intervals is wider in the Salinello valley (Figs. 1B, 2A). In the Corano Quarry location, dolomitization occur in the Calcare Massiccio and Bugarone Formations only as meter-sized dolostone geobodies in the footwall of the Montagna dei Fiori Fault (Fig. 4).

Dolostone breccias in fault cores is typically clast-supported, with angular and millimeter- to centimeter-sized fragments (Fig. 3C), changing to crackle breccia (Woodcock and Mort, 2008) away from the master slip surface. In the proximity of the master slip surface, dolostone fragments are sporadically overprinted by millimeter-sized dolomite veins. The breccia fragments, where cemented, are commonly surrounded by calcite.

Dolomitization does not follow a systematic pattern. In some outcrops, dolomitization fronts show irregular outlines following, but also cross-cutting, the bedding surfaces (Fig. 5). Dolomitized intervals vary in thickness from few meters to hundred meters affecting the totality of the exposed Calcare Massiccio and only the lower part of Corniola Formation, where no clay interlayers are present. Dolomitized intervals in the Corniola Formation have a darker color relative to the host rock and are systematically more fractured than the hosting limestone. High amplitude (> 1 mm) bed-parallel stylolites are clearly visible in both limestones and dolostones

Solid Earth Discuss., https://doi.org/10.5194/se-2018-136
Manuscript under review for journal Solid Earth
Discussion started: 3 January 2019
© Author(s) 2019. CC BY 4.0 License.



(Fig. 5). However, in some dolostones only ghosts of stylolite traces can be seen. The dolostones locally contain porosity, appearing as millimetre- to centimetre-sized pores.

## 4.2 Petrography

### 4.2.1 Early calcite cementation

The early diagenetic products in the studied intervals are generally non-ferroan calcite cements. The first calcite cements precipitated following a phase of bioclast micritization (*sensu* Bathurst, 1975) in grain supported intervals. In chronological order, they include: 1) fibrous cements (FC) riming the bioclasts, mostly in the peloidal facies of the Calcare Massiccio Formation (Fig. 6A). These cements are dull to non-luminescent under cathodoluminescence; 2) mosaic cements (MC), commonly fill the intergranular pore spaces (Fig. 6B), and also occur as syntaxial overgrowths on echinoderm fragments. These cements exhibit deformation twining and show well-developed dull and orange concentrically-zoned cathodoluminescence pattern (Figs. 6C and D). They contain only mono-phase all-liquid inclusions. All of these cements are postdated by high amplitude bed-parallel stylolites.

### 4.2.2 Dolomitization

All the dolomite types are non-ferroan and dominantly fabric destructive. The two first dolomite types (D1 and D2) are the dominant dolomite types in the studied outcrops. These dolomites are distributed within the damage zones of the ~ N-S and E-W Jurassic rift-related extensional faults and, in places, displaced by them (Fig. 2A, site 1). The third and fourth dolomite types (D3 and D4) are mainly observed within the damage zone of the Montagna dei Fiori Fault (NNW-SSE), and appear only as dolomitic pockets overprinting D1 and D2 at the proximity of the ~ N-S and E-W extensional faults. The fifth dolomite type (D5) is found only within the brecciated zones associated with the Montagna dei Fiori Fault damage zone. The distinctive petrographic features of the recognized dolomite types are summarized below:

**Dolomite 1 (D1)** is a replacive dolomite which commonly appears as dispersed rhombs and aggregates, and locally rims fracture walls cemented by calcite (CV1) (Figs. 6E and F). D1 postdates the micritic envelopes and early calcite cements, and predates high amplitude bed-parallel stylolites (Figs. 6G and H). The crystals are fine to medium sized (< 350 μm) and consists of relatively turbid, solid-inclusion rich, well-developed euhedral to subhedral crystals, with red luminescence, occasionally developing a concentrical zonation.

Solid Earth Discuss., https://doi.org/10.5194/se-2018-136
Manuscript under review for journal Solid Earth
Discussion started: 3 January 2019
© Author(s) 2019. CC BY 4.0 License.



**Dolomite 2 (D2)** is a replacive dolomite (Figs. 7A and B), infrequently occluding existing pore spaces. Like D1, it also frequently predates high amplitude bed-parallel stylolites (Figs. 6G and H. D2 generally exhibits a tightly packed texture with no or little intercrystalline porosity. The crystals are medium to coarse sized (≤ 500 μm) including a turbid core followed by a transparent subhedral to anhedral rim and trace quantities of saddle dolomite developing swiping extinction. In some crystals one additional turbid zone rich in solid and fluid inclusions is present. Cathodoluminescence observations enabled to recognize the presence of D1 in their turbid cores. D2 crystals are characterized by zones of bright red-pink luminescence separated by purple luminescence zones.

**Dolomite 3 (D3)** is present as small localized bodies in the Calcare Massiccio (at the Castel Manfrino reference section), in the Corniola Formation (at the Osso Caprino Road), and in the Calcare Massiccio and Bugarone Formations (at the Corano Quarry). In the Corano Quarry the dolomitized Bugarone and Calcare Massiccio Formations are in the footwall of the Montagna dei Fiori Fault; and juxtaposed to the undolomitezed, intensely foliated Scaglia Formation (the hanging wall). Within the Bugarone Formation in this fault damage zone, D3 locally cements the millimeter-sized angular breccias that are in turn affected by fault parallel stylolites (Figs. 7C and D). The SEM and BSEM analysis performed on the samples from the immediate adjacent Scaglia Formation within the aforementioned fault damage zone did not indicate the presence of any dolomite in this formation. D3 crystals are mostly transparent euhedral to anhedral (< 300 μm), with minor development of saddle morphologies in larger crystals (> 500 μm) (Figs. 7E to H). The euhedral to anhedral crystals are generally replacive, displaying a faint core, which compared to previous dolomite types has fewer solid inclusions. The saddle crystals are occasionally replacive but majorly appear as cement in fractures. They display typical curved and slightly serrated crystal terminations with swiping extinction. These saddle dolomites were only observed in the Castel Manfrino reference section. D3 generally exhibit a dull purple color with bright orange zones and subzones in core and/or rims when viewed under cathodoluminescence (Figs. 7E to H).

**Dolomite 4 (D4)** appears as a matrix replacive and dolomite cement surrounding porosity and locally recrystallizing D1 and D2 (Figs. 8A to F). D4 also occludes bed parallel shear fractures and appears along the bed parallel stylolites (Figs. 9A to D). In the Castel Manfrino reference section, some intercrystalline vuggy porosity is filled with fine dolomite rhombs including D4

Solid Earth Discuss., https://doi.org/10.5194/se-2018-136
Manuscript under review for journal Solid Earth
Discussion started: 3 January 2019
© Author(s) 2019. CC BY 4.0 License.



with relics of D2 within their core (Figs. 8E and F). The porosity may be preserved or partially to completely filled by CV4. D4 crystals have a turbid, solid-inclusion rich core and transparent rim. They are fine to medium sized (< 200-350 μm), presenting subhedral to infrequent euhedral crystals. D4 exhibits a distinct luminescence pattern including a purple zone and an irregular green subzone.

**Dolomite 5 (D5)** occurs as crystals cementing micro-veins that cross-cut precursor dolomite types including dolomitic breccia fragments. In cemented breccias, D5 is postdated by CV3. D5 is transparent, anhedral and is characterized by a bright red luminescence (Figs. 9E and F).

### 4.2.3 Late calcite cementation

Four generations of calcite veins postdating dolomitization have been identified (Figs. 10 and 11): 1) Calcite vein 1 (CV1) occurs only in Calcare Massicio limestones and is represented as centimeter-sized, strata-bound, bedding-perpendicular veins with irregular fracture walls, exhibiting white color in the outcrops. They postdate the first dolomite type (D1) riming the same fractures that abut the high amplitude bed parallel stylolites. CV1 often show blocky to elongated crystal morphologies and displays well-developed deformation twinning planes (Type II of Burkhard, 1993). This calcite exhibits concentrical zonation and dull zones alternate with orange luminescence zones (Figs. 11A and B). 2) Calcite vein 2 (CV2) exclusively occurs in the intensely deformed Scaglia Formation within the fault damage zones and correspond to tension gashes associated with stylolites (*sensu* Nelson, 1981). CV2 veins are mostly recorded in foliated shear deformation zones with well-defined S-C fabrics, exhibiting blocky, elongated to fibrous shapes with strongly developed tightly spaced deformation twinning planes (Type II of Burkhard, 1993). CV2 displays yellow to orange luminescence with locally darker sector zones. The yellow to orange luminescence characteristic of CV2 is comparable with those of encasing Scaglia host rocks (Figs. 11C and D). 3) Calcite vein 3 (CV3) occurs as cement, filling the extensional faults master plane and isolated veins within the extesional fault damage zones. CV3 cements the brecciated fault-infillings containing angular fragments of host rock limestones, dolostones and earlier calcites. In the brecciated zones at the backlimb of the anticline (Montagna dei Fiori Fault), CV3 postdates the last dolomitization phase (D5) with no evidence of physical disruption. CV3 exhibits a white to translucent color in hand specimen. The crystals are blocky with no or weakly developed deformation twinning planes, and are characterized by a dark orange to brown luminescence with distinct darker sector zones (Figs. 11E and F). 4)

Solid Earth Discuss., https://doi.org/10.5194/se-2018-136
Manuscript under review for journal Solid Earth
Discussion started: 3 January 2019
© Author(s) 2019. CC BY 4.0 License.



Calcite vein 4 (CV4) exists as isolated veins, pore-filling as well as breccia cements postdating all the preceding dolomites and calcites. The breccia fragments are more often dolostones. CV4 has a white to translucent white color in hand specimen with blocky crystal morphology and no evidence of subsequent deformation (e.g. deformation twining planes), and is characterized by distinct concentrical zonation (Figs. 11G and H).

### 4.3 Geochemistry

#### 4.3.1 Carbon and oxygen stable isotopes

The carbon and oxygen stable isotopic data ($\delta^{13}C$ and $\delta^{18}O$) of host rocks, dolomites and calcites are given in Table 1 and shown in Figures 12A and B. The marine stable isotopic compositions reported by Veizer et al. (1999) were used as marine reference values. Accordingly, Lower Jurassic marine limestones are characterized by $\delta^{13}C$ values of -0.5 to +4.5‰ and $\delta^{18}O$ values of -2.5 to +1.0‰ V-PDB. The $\delta^{18}O$ values of the marine dolomites are known to be 3-4‰ V-PDB more enriched than those of co-genetic marine limestones (Land, 1980; Major et al., 1992; Horita, 2014). Both $\delta^{13}C$ and $\delta^{18}O$ values of the host rocks are within the expected range of the Lower Jurassic marine limestones but the Corniola host rocks show slightly lower values comparing to those of Calcare Massiccio. In the Calcare Massiccio host rocks, the $\delta^{13}C$ values plot between +2.4 and +3.1‰ and $\delta^{18}O$ values are within the range of -1.6 and 0.0‰ V-PDB. The $\delta^{13}C$ values in the Corniola host rocks are +2.0 and +2.5‰ while the $\delta^{18}O$ values are -3.1 to -1.4‰ V-PDB. The $\delta^{13}C$ and $\delta^{18}O$ values of the Scaglia host rocks range between +1.0 to +3.3‰ for $\delta^{13}C$ and -2.2 to -1.0‰ V-PDB for $\delta^{18}O$. The obtained values are characterized in the mean range of Upper Cretaceous to Paleogene marine limestones (Veizer et al., 1999; +1.0 to +4.5‰ for $\delta^{13}C$ and -4.0 to +2.0‰ V-PDB for $\delta^{18}O$).

The $\delta^{13}C$ values of CV1 are between +1.6 and +2.1‰ which plot within the range of reference values (Jurassic) but are slightly lower than the surrounding host rock values. The $\delta^{18}O$ values are between -4.7 and -2.7‰ V-PDB which are lower than those of reference and host rock values.

The $\delta^{13}C$ values of all dolomite types (+0.6 to +3.4‰) fall within the range of host rocks and Jurassic marine limestones (Veizer et al., 1999). The $\delta^{18}O$ shows a wider range of values, somehow overlapping but also lower than those of host rocks (-4.5 to -0.9‰ V-PDB) and the presumable Lower Jurassic marine dolomites. The majority of values plot between -3.5 and -1.5‰ V-PDB. The small size and overgrowth nature of certain dolomite types (e.g. D2 and

Solid Earth Discuss., https://doi.org/10.5194/se-2018-136
Manuscript under review for journal Solid Earth
Discussion started: 3 January 2019
© Author(s) 2019. CC BY 4.0 License.



D5) limits their proper isolation for geochemical analyses. Only one sample from D1 dolomite could be measured for $\delta^{13}C$ and $\delta^{18}O$ values, showing +2.5 and -1.9‰ V-PDB, respectively. The $\delta^{13}C$ and $\delta^{18}O$ values of D3 dolomite range from +2.0 to +2.6‰ and -2.8 to -1.9‰ V-PDB, respectively, with values lower than those of the host rock.

D4 dolomite has $\delta^{13}C$ values between +2.4 and +2.5‰, and $\delta^{18}O$ values of -3.0 to -2.5‰ V-PDB. The $\delta^{13}C$ and $\delta^{18}O$ values of CV2 are +1.2 to +3.1‰ and -1.7 to -1.7‰ V-PDB, respectively. The $\delta^{13}C$ values of CV3 are between +0.5 and +2.4‰, and the $\delta^{18}O$ values cover a range of -2.2 to 0.0‰ V-PDB. The $\delta^{13}C$ and $\delta^{18}O$ values of CV4 are +3.8 to +4.9‰ and -9.4 to -9.1‰ V-PDB, respectively. The $\delta^{13}C$ values are slightly higher but the $\delta^{18}O$ values are considerably lower compared to preceding calcite generations and the measured values from host rocks.

#### 4.3.2 $^{87}Sr/^{86}Sr$ ratios

Samples from host rocks (i.e. Calcare Massiccio and Corniola Formations), dolomites (D1, D3 and D4) and the Scaglia Formation in juxtaposition with the dolostones were analyzed for their $^{87}Sr/^{86}Sr$ isotopic ratios. The obtained ratios versus $\delta^{18}O$ values of the analyzed samples are shown in Fig. 12C. The $^{87}Sr/^{86}Sr$ ratios obtained from the Calcare Massiccio and Corniola limestones are 0.70766 and 0.70725 (n = 2), respectively, which is in agreement with the values of the Lower Jurassic marine carbonates (0.70704-0.70768) reported by McArthur et al. (2012). CV1 show a value equal to 0.70773.

All the dolomite types display higher $^{87}Sr/^{86}Sr$ ratios when compared to the host rocks and reference values of the Lower Jurassic marine carbonates. D1 (replacive) and D4 cements show a comparable narrow range with values between 0.70784 and 0.70790, respectively. While, the two D3 samples (replacive and cement) display higher $^{87}Sr/^{86}Sr$ ratios (0.70858 and 0.70963, respectively). The $^{87}Sr/^{86}Sr$ ratios obtained for dolomites do not show co-variation with corresponding $\delta^{18}O$ values. The radiogenic Sr analysis was not performed on D2 and D5 since the physical mixing with other dolomite types could not be avoided.

The $^{87}Sr/^{86}Sr$ ratios of the two samples of Scaglia Formation are 0.70784 to 0.70790. The CV2 veins in Scaglia Formation show comparable ratios of 0.70779 and 0.70787. These values fit within the limits of values assigned by McArthur et al. (2012) for the Cenomanian-Bartonian (Scaglia age) marine carbonates (0.70730-0.70790).

Solid Earth Discuss., https://doi.org/10.5194/se-2018-136
Manuscript under review for journal Solid Earth
Discussion started: 3 January 2019
© Author(s) 2019. CC BY 4.0 License.



400 **4.4 Fluid inclusion microthermometry**

401 The overview of microthermometry measurements is given in Table 1 and Figs. 13A to
402 C. On the basis of optical microscopy analysis of wafers, D1 contain dominantly mono-phase
403 aqueous inclusions with sizes greater than 5 µm. It is common for small inclusions (< 3 µm) to
404 remain mono-phase all liquid at room temperature due to their metastability (Goldstein and
405 Reynolds, 1994). Thus, to eliminate the possible role of metastability, the samples were placed in
406 a freezer for several days following the procedures described in detail by Goldstein and Reynolds
407 (1994). All liquid inclusions remained unchanged and no vapor bubble was developed within
408 them, which discards the metastability effect.

409 In order to properly observe the phase transitions in the all liquid inclusions, they were
410 rapidly heated up to ~ 200°C to stretch and nucleate a bubble at room temperature (Goldstein,
411 1990). All the inclusions froze at -65 to -49°C. The first melting (Te) was detected between -22
412 to -19.3°C. The final ice melting (Tm) appeared at temperatures between -7.7 and -2°C.
413 Applying Bodnar´s (1993) equation, the obtained final melting temperatures correspond to
414 salinity ranges of 3.5 to 11.3 eq. wt. % NaCl.

415 D2 is characterized by the presence of mono-phase and infrequent two-phase inclusions
416 generally within their growth zones. The homogenization temperature of two-phase inclusions
417 varies between 58 and 71°C. Upon cooling, a complete freezing of the fluid phase is reached
418 at -56 to -40°C. The first ice melting temperature was distinguished at -22°C. The final ice
419 melting temperatures fall within -17.5 and -5°C, corresponding to salinities between 7.9 and
420 20.5 eq. wt. % NaCl.

421 D3 is commonly inclusion poor. The measureable inclusions were detected and examined
422 only in saddle dolomite crystals. These crystals contain only two-phase aqueous inclusions. Their
423 homogenization temperatures are within the narrow range of 70 to 73°C. The complete freezing
424 and first ice melting temperatures could not be distinguished but the final ice melting
425 temperature occurred at temperatures between -13 and -6°C equal to salinity ranges of 9.2 to
426 16.9 eq. wt.% NaCl. The first melting temperatures of fluid inclusions in D1, D2 and D3 were
427 about -21°C, suggesting a $H_2O$-NaCl fluid system.

428 D4 contains only two-phase aqueous inclusions. The homogenization temperatures in D4
429 vary between 79 and 105°C. Complete freezing of inclusions occurred at temperatures
430 between -86 and -54 °C. The first ice melting was detected at -35 to -40°C indicating the

Solid Earth Discuss., https://doi.org/10.5194/se-2018-136
Manuscript under review for journal Solid Earth
Discussion started: 3 January 2019
© Author(s) 2019. CC BY 4.0 License.



possible presence of divalent cations such as $Ca^{2+}$ and/or $Mg^{2+}$ in the fluids (Shepherd et al., 1985; Goldstein and Reynolds, 1994). The final ice melting temperatures fall within a range of -15 and -9°C corresponding to salinities of 12.8 to 18.6 eq. wt. % NaCl. A couple of inclusions show homogenization temperatures exceeding 120°C with salinities higher than 20 eq. wt. % NaCl. The inconsistent homogenization temperatures and salinities obtained for these fluid inclusions, within the framework of an individual fluid inclusion assemblage (FIA) described by Goldstein and Reynolds (1994), indicate possible re-equilibration of these inclusions and thus are not used in the interpretations.

The obtained homogenization temperatures in all fluid inclusion assemblages indicate the minimum temperatures at which the fluids could have been trapped (Goldstein and Reynolds, 1994). No correction was made for pressure effects on entrapment temperatures since no data regarding the exact depth and pressure of entrapment are available. In absence of independent thermal indicators such as Conodont Alteration Index (CIA) and Vitrinite Reflectance (VR), the accuracy of pressure correction cannot be well constrained (Slobodník et al, 2006), and thus no correction was made for pressure effects on homogenization temperatures.

No measurable fluid inclusion could be identified in CV1 and CV2 due to intense deformation twinning. CV3 and CV4 contain only primary mono-phase aqueous inclusions, indicating an entrapment temperature of below about 40-50°C (Goldstein and Reynolds, 1994). A complete freezing of the inclusions in CV3 occurred at temperatures between -40 and -52.5°C. The first melting temperature was detected at about -21 to -22°C, suggesting a $H_2O$-NaCl composition. The final melting temperatures range between -6.4 and -2.7°C, corresponding to salinities between 9.7 and 4.5 eq. wt. % NaCl. The majority of the values cluster between 7.8 and 5 eq. wt. % NaCl.

The complete freezing temperatures of the inclusions in CV4 fall within -46 and -35.5°C. The first melting temperature could not be determined with confidence but the final melting temperatures were reached at about -0.1 to -1.8°C, corresponding to salinities of 0.17 to 3.0 eq. wt. % NaCl.

## 5 Discussion

### 5.1 Stable and radiogenic isotopic composition of the parental fluids

The $\delta^{13}C$ values of all dolomite types mimic the range of host rock and Jurassic marine limestones and, consequently, they can be interpreted as largely rock-buffered. Their $\delta^{18}O$ values

Solid Earth Discuss., https://doi.org/10.5194/se-2018-136
Manuscript under review for journal Solid Earth
Discussion started: 3 January 2019
© Author(s) 2019. CC BY 4.0 License.



462 are partly comparable to those of their respective host rocks as well as Jurassic marine reference
463 values but more depleted when compared to the presumable Jurassic marine dolomites. The
464 relatively depleted $\delta^{18}O_{dolomite}$ values could indicate the contribution of heated fluids in
465 dolomitization process, although it could also relate to recrystallization of a precursor dolomite
466 by fluids at higher temperature or $^{18}O$-depleted (Land, 1980; 1985). The absence of distinctive
467 textural evidence in the analyzed samples such as enlarged crystal size and/or systematic mottled
468 cathodoluminescence pattern, and their co-variation with $\delta^{18}O$ values do not confirm
469 recrystallization (Mazzullo, 1992 and ref. therein). Nevertheless, special care was taken to avoid
470 the samples that occasionally displayed scattered mottled luminescence.
471 The oxygen isotope fractionation relation between water and dolomite (Land, 1983) was
472 used to determine the most plausible parental fluids. In order to avoid erroneous results due to
473 rock-buffered $\delta^{18}O$ values, only the $\delta^{18}O$ values of dolomite cements, especially from the bed
474 parallel veins containing D4 were used. These values may provide the closest approximation to
475 the $\delta^{18}O$ signature of the parental fluids (Barker and Cox, 2011). Accordingly, a $\delta^{18}O$ value of ≈
476 +2.5 to +4‰ V-SMOW was calculated for D3, while this values increase to ≈ +5 to +7.5‰
477 V-SMOW for D4 (Fig. 13D). The calculated compositions of the potential parental fluids are
478 progressively higher The higher $\delta^{18}O$ composition of the dolomitizing fluids relative to the
479 Mesozoic seawater, which is estimated at -1.2 to -1‰ V-SMOW (Shackleton and Kennett, 1975;
480 Marshall, 1992; Saelen et al., 1996), is compatible with fluids derived from or that had interacted
481 with siliciclastics, crystalline basement (Taylor, 1997) and/or evaporite-derived brines.
482 The $^{87}Sr/^{86}Sr$ ratios obtained for all dolomite types are higher than the Lower Jurassic
483 marine carbonate values (0.70704-0.70768; McArthur et al., 2012). Since marine carbonates
484 have very low rubidium (Rb) concentrations they produce negligible *in situ* radiogenic $^{87}Sr$ after
485 their deposition (Stueber et al. 1972; Burke et al. 1982). Therefore, the higher $^{87}Sr/^{86}Sr$ ratios can
486 be explained by the contribution of fluids originated or interacted with potassium rich
487 siliciclastics (K-feldspars), crystalline basement and/or stratigraphic levels with higher $^{87}Sr/^{86}Sr$
488 ratios (Emery and Robinson 1993; Banner, 2004). Taking into account that the Upper Triassic
489 Burano Formation underlying the studied intervals has $^{87}Sr/^{86}Sr$ ratios between 0.70774 and
490 0.70794 (Boschetti et al., 2005), the $^{87}Sr/^{86}Sr$ ratios (D1 and D4) can partially be explained by
491 their contribution. However, this contribution cannot justify much higher $^{87}Sr/^{86}Sr$ ratios
492 recorded in D3, being higher than values reported for Phanerozoic seawater (McArthur et al.,

Solid Earth Discuss., https://doi.org/10.5194/se-2018-136
Manuscript under review for journal Solid Earth
Discussion started: 3 January 2019
© Author(s) 2019. CC BY 4.0 License.



2012), and the values recorded in adjacent basinal deposits (i.e. Corniola and Scaglia Formations). Therefore, parental fluids most likely originated from or had interacted with the siliciclastics underlying the Burano Formation (Verrucano Formation), if present, and/or with the crystalline basement with common elevated $^{87}Sr/^{86}Sr$ ratios (0.71500-0.72650; Del Moro et al., 1982).

CV1 is characterized by $\delta^{13}C$ and $\delta^{18}O$ values lower than the host limestones (i.e. Calcare Massiccio), while its $^{87}Sr/^{86}Sr$ ratio is comparable to them. The salinity and composition of the parental fluids cannot be inferred here since no measurable fluid inclusions were found within this cement. The $^{87}Sr/^{86}Sr$ ratio being within the range of the corresponding host rocks and the reference values, points to a rock-buffered system for $^{87}Sr/^{86}Sr$.

The $\delta^{13}C$ and $\delta^{18}O$ values obtained for CV2, as well as $^{87}Sr/^{86}Sr$ ratios, fall within the range of the Scaglia host rocks, thus reflecting their rock-buffered nature. This interpretation is further supported by the comparable luminescence characteristics of CV2 with that of encasing Scaglia host rocks. The fluids from which CV2 calcite precipitated were most likely derived from carbonate dissolution during pressure-solution and stylolitization.

CV3 is characterized by $\delta^{13}C$ values within the Jurassic marine values but are generally lower than the host rocks, while their $\delta^{18}O$ values partially overlap both the hosting limestones and dolostones. Microthermometry of fluid inclusions revealed only mono-phase aqueous inclusions and thus precipitation at relatively low temperature ($\leq$ 40-50°C) with moderate salinity (4.5-9.7 eq. wt. % NaCl). Such levels of salinity can be assigned to evaporated seawater, residual brines or fluids derived from evaporite dissolution, and thus makes it difficult here to interpret their exact origin with the available data.

CV4 is the latest calcite phase, and records the $\delta^{13}C$ and $\delta^{18}O$ values, respectively enriched and significantly depleted when compared to their hosting rocks and preceding diagenetic products. Generally, the enrichment of $^{13}C$ could suggest $CO_2$ outgassing due to evaporation (Friedman, 1970; Hendry et al., 2015) or bacterial fermentation (methanogenesis) of organic matter (Hudson, 1977) in low temperature diagenetic environments. The homogenization temperature of CV4 being below about 40-50°C could support any of these processes. Their low $\delta^{18}O$ values and fluid inclusions with salinities comparable to, but also significantly lower than, seawater reflect the contribution of meteoric fluids during precipitation of this calcite.

### 5.2 Origin of the dolomitizing fluids

Solid Earth Discuss., https://doi.org/10.5194/se-2018-136
Manuscript under review for journal Solid Earth
Discussion started: 3 January 2019
© Author(s) 2019. CC BY 4.0 License.



524 The contribution of brines that derived from highly evaporated seawater or evaporites is
525 suggested by the elevated salinity values obtained from microthermometry of the fluid inclusions
526 (3.5 to 20.5 eq. wt. % NaCl). Accordingly, two sources that could potentially provide such fluids
527 can be proposed: 1) fluids related to the Late Messinian evaporites, associated with the overlying
528 Laga Formation, deposited during the Upper Miocene time, and their possible downward
529 percolation through fault zones by density driven flow and/or seismic pumping mechanisms
530 (Sibson, 1981; McCaig, 1988, 1990); or their tectonic involvement into the Apenninic thrust
531 wedge during its propagation (underthrusting; Lobato et al., 1983); and 2) fluids related to the
532 underlying décollement horizon of Burano evaporites (Upper Triassic) and their upward flow
533 through fault zones during development of the Montagna dei Fiori Anticline. The first scenario is
534 valid if the dolomitization would have occurred only from the Upper Miocene time onwards.
535 Several researchers (e.g. Vai and Ricci Lucchi, 1977; Bassetti et al., 1998; Roveri et al. 2001)
536 have shown that the occurrence of primary shallow-water evaporites, which were dominantly
537 gypsum, was limited to the western and central parts of the northern Apennines consisting of
538 thrust-top marginal basins. In contrast, evaporites never precipitated in parts of the central
539 Apennines including the Montagna dei Fiori region (Marche area) (Roveri et al. 2001). Hence,
540 the evaporitic horizons existing within the Laga Formation corresponds to resedimentation
541 (gypsum debris) of those previously precipitated in the marginal basins. This interpretation
542 makes the Messinian evaporites an unlikely source of Mg-rich brines. Moreover, taking into
543 account that the maximum burial related temperature of the Calcare Massiccio Formation did not
544 exceed 80°C in the Montagna dei Fiori region (Ronchi et al., 2003), it's not likely that the
545 downward percolation of relatively low-temperature brines derived from the Messinian
546 evaporites, located at the higher stratigraphic levels, could reach or exceed the high temperatures
547 recorded in fluid inclusions of the dolomites in the Calcare Massiccio Formation (D4; up to
548 105°C), given that the homogenization temperatures reflect the minimum entrapment
549 temperatures (Goldstein and Reynolds, 1994). Deep circulation of these brines, if existed, can
550 also be excluded by their limited tectonic involvement within the thrust wedge being confined
551 merely to the off shore wards of the Montagna dei Fiori region (Artoni, 2013).
552 Accordingly, the Upper Triassic Burano Formation appears as the most plausible source
553 for the high salinity brines recorded in fluid inclusions, and likewise, the Mg-rich fluids could
554 have been originated from post-evaporite brines associated with them (Carpenter, 1978;

Solid Earth Discuss., https://doi.org/10.5194/se-2018-136
Manuscript under review for journal Solid Earth
Discussion started: 3 January 2019
© Author(s) 2019. CC BY 4.0 License.



McCaffrey et al., 1987). The fluctuations in salinity may argue for different degrees of contribution of pore waters of lower salinity (e.g. marine or meteoric).

### 5.3 Timing and structural controls on the evolution of parental fluids

A generalized paragenesis and the relative chronology of dolomitization in relation to the structural evolution of the Montagna dei Fiori Anticline are illustrated in Figs. 14 and 15. The paragenesis is constructed on the basis of direct evidences recorded during observations at outcrop scale and microscopic observations (e.g. cross-cutting relationships between diagenetic phases, stylolites, fractures and other structural kinematics), and indirect evidences (e.g. regional geodynamics and burial history).

The occurrence of micritic envelopes and fibrous calcite cements (FC), in grain supported stratigraphic levels of the Calcare Massiccio Formation, is interpreted to be of eogenetic origin (i.e. marine phreatic diagenesis; Moore, 1989), reflecting an early diagenesis shortly after deposition. The well-developed dull and orange concentric cathodoluminescence pattern of the succeeding mosaic calcite cement (MC) suggests a progressive shift to more reducing conditions during precipitation in a phreatic diagenetic environment (as shown in Li et al., 2017). High amplitude bed parallel stylolites postdate both cements, which confirm their precipitation before significant burial. The observations made here are in agreement with earlier work by Giacometti and Ronchi (2000), interpreting that the Calcare Massiccio Formation was cemented during the early diagenetic stages.

D1, CV1 and D2 are postdated by well-developed, high amplitude bed-parallel stylolites. Presence of D1 and CV1 in bed-perpendicular veins typically abutted by these stylolites (see Figs. 6E to H) support the interpretation that the first dolomitization event (D1 and D2) took place before significant burial and stylolite development, being the latter and bed-perpendicular veins dynamically compatible within the same stress field characterized by a vertical, load-related maximum principal axis of the stress ellipsoid. The dominantly mono-phase fluid inclusions within D1 and D2 are in agreement with precipitation temperatures below about 40-50°C, suggesting a relatively shallow to intermediate burial environment and hence supporting a pre-Apenninic orogeny age of precipitation from a mix of formational and extra-formational fluids with elevated $^{87}Sr/^{86}Sr$ ratios. The distribution of D1 and D2 nearby the rifting-related ~ N-S and E-W striking extensional faults and even their displacement along them (Fig. 2A, e.g. site 1), point to the possible contribution of these faults in occurrence of D1 and

Solid Earth Discuss., https://doi.org/10.5194/se-2018-136
Manuscript under review for journal Solid Earth
Discussion started: 3 January 2019
© Author(s) 2019. CC BY 4.0 License.



D2. These faults dominantly affect the Jurassic rocks older than the Maiolica Formation which is attributed to the post-rift deposits, therefore suggesting a pre-Maiolica age for these dolomite types. Although, an absolute age cannot be provided, based on the evidence discussed above, the circulation of Mg-rich fluids during this dolomitization event was most likely controlled by rifting-related Jurassic extensional fault zones cutting through the crystalline basement. Taking into account that D1 and D2 are the volumetrically more relevant dolomites within the studied intervals, and assuming the likely role of syn-rift extensional faults (Early to Late Jurassic) in their precipitation, a dominantly syn-rift dolomitization process is proposed for the dolostones in the Montagna dei Fiori Anticline.

D3 and D4 both record elevated $^{87}Sr/^{86}Sr$ ratios which accounts for their fault-controlled origin. However, their occurrence at the top of the Calcare Massiccio and overlaying Bugarone Formation (Corano Quarry site) which is < 1 m thick in Montagna dei Fiori region, and is marked as the final rift deposit (Cardello and Doglioni, 2015) discards a syn-rift origin for these dolomites. Moreover, D3 and D4 postdate the development of high amplitude bed parallel stylolites. The formation of stylolites requires an approximate overburden of 600 to 1500 m (Lind, 1993; Machel, 1999; Mountjoy et al., 1999; Schulz et al., 2016), corresponding to a late to post-Maiolica deposition time (Early Cretaceous time onwards). The presence of D3 and D4 dolomites in bed parallel fractures and shear veins (D4) suggests their association with contractional deformations, i.e. the most likely tectonic regime for explaining bed-perpendicular dilation. Therefore, the volumetrically minor second stage of dolomite precipitation may possibly be related to the Late- to post-Miocene compressional tectonics recorded in this region (e.g. Mazzoli et al., 2002; Artoni, 2013; Storti et al., 2018).

Dolostones containing D3 and D4 appear commonly as clast-supported breccias along fault zones pertaining to the Montagna dei Fiori Fault, then overprinted by fault-parallel stylolites. Accordingly, the occurrence of these dolomites was probably synchronous with the incipient stages of fault development, predating fault buttressing (Storti et al., 2018). Homogenization temperatures recorded in D4 (up to 105°C), much higher than the maximum temperatures recorded in the host rocks (below about 80°C; Ronchi et al., 2003), suggest hydrothermal fluid circulation. The development of the Montagna dei Fiori Anticline at the toe of the Late Miocene Central Apennines thrust wedge could have favored the forelandward migration of hydrothermal fluids expelled from the more internal regions of the belt, similarly to

Solid Earth Discuss., https://doi.org/10.5194/se-2018-136
Manuscript under review for journal Solid Earth
Discussion started: 3 January 2019
© Author(s) 2019. CC BY 4.0 License.



what has been proposed for the Rocky Mountains foreland (i.e. squeegee flow model; Machel and Cavell (1999). Such a migration may have possibly favored the precipitation of D4 in bed parallel veins, generally considered as evidence for syn-compressional fluid overpressure (Sibson, 2001; Hiemstra and Goldstein, 2015). The presence of D5 only within the damage zone of the Montagna dei Fiori Fault, postdating dolostone brecciation and, in places, cementing breccia fragments, may suggest that D5 dolomite precipitation was associated with the late stage evolution of the Montagna dei Fiori Fault, predating late stage calcite precipitation.

The presence of several generations of bed perpendicular stylolites bounding and intersecting CV2 veins, supports that late stage calcite cements precipitated closely associated with the deformation history of the Scaglia Formation in the hanging wall of the Montagna dei Fiori Fault, during buttressing against Calcare Massiccio and Corniola Formations in the footwall, and related with the positive inversion event induced by thrust-sheet stacking at depth (Storti et al., 2018). Precipitation of CV3 and CV4 in interpreted to have occurred during uplift and cooling as revealed by their relatively low homogenization temperatures (≤ 40-50°C). Deformation twining is either absent or weakly developed, reflecting the lack of significant tectonic deformation after calcite precipitation. These cements postdate the dolomitization events, high amplitude bed perpendicular and parallel stylolites, and are precipitated as cements bounding the breccia fragments within the damage zone of the Montagna dei Fiori Fault. Salinities calculated from their fluid inclusions, particularly in CV4 suggests precipitation from meteoric waters, which should have been favored during the late evolutionary stages of antiformal stacking beneath the Montagna dei Fiori Anticline, and eventual late extensional slip along the Montagna dei Fiori Fault (Storti et al., 2018). The results obtained in this study are in relative agreement with the earlier work by Ronchi et al. (2003) and Murgia et al. (2004) in the Central Apennines, assigning dolomitization phases to the pre- and syn-orogenic deformations, although they did not specify the direct relation between the structures and the different types of dolomite.

## 6 Conclusions

The Lower Jurassic limestones outcropping at the core of the Montagna dei Fiori Anticline (Central Apennines, Italy) are massively affected by dolomitization, in damage zones of the pre-orogenic faults inherited from the Tethyan rifting and the ones formed during the Apenninic orogeny. Cross-cutting relationships between deformation structures, and results from

© Author(s) 2019. CC BY 4.0 License.

optical and cold cathodoluminescence petrography, fluid inclusion microthermometry, and isotope geochemistry, support the occurrence of two major dolomitization events. The first event is interpreted as developed during the late stages of Tethyan rifting in Jurassic and resulted in volumetrically significant dolostone geobodies. These dolostones are majorly matrix replacive and their precipitation initiated prior to the significant burial as reflected in their cross-cutting relationship with bed parallel stylolites, and by homogenization temperatures in fluid inclusions that are dominantly below about 40-50°C. The second dolomitization event corresponds to volumetrically less relevant replacive dolomite and dolomite cements occluding fractures. These dolomites precipitated during hydrothermal fluid circulation associated with contractional tectonics during the Apenninic orogeny, possibly at the onset of the growth of the Montagna dei Fiori Anticline (Late Miocene).

Dolomitizing fluids in both events were most likely sourced from evaporitic brines associated to the underlying Burano evaporites and their interaction with siliciclastics and/or the crystalline basement.

*Author contributions.* M. Mozafari participated in fieldwork, performed petrographic and microthermometric analyses, provided their interpretation, and wrote the manuscript; R. Swennen participated in fieldwork, discussed the results of the diagenetic study, and critically reviewed the manuscript; F. Balsamo contributed to collect and interpret structural data, discussed structural diagenesis data interpretation, and critically reviewed the manuscript; H. El Desouky collected $^{87}Sr/^{86}Sr$ data; F. Storti conceived the research, contributed to collect and interpret structural data, discussed structural diagenesis data interpretation, and critically reviewed the manuscript; C. Taberner participated in fieldwork, discussed the results of the diagenetic study and their framing into the proposed structural evolution, and critically reviewed the manuscript.

*Acknowledgments*. This research was performed by collaboration between Parma and KU Leuven universities in the framework of a research project (PT12432 and GFSTE 1100942) funded by Shell Global Solutions International (Carbonate Research Team, now Geology and New Reservoir Types Team). We thank E.M. Selmo (Parma University) and M. Joachimski (University of Erlangen, Germany) for the stable carbon and oxygen analysis. G. Davis (VU

Solid Earth Discuss., https://doi.org/10.5194/se-2018-136
Manuscript under review for journal Solid Earth
Discussion started: 3 January 2019
© Author(s) 2019. CC BY 4.0 License.

679 Amsterdam, the Netherlands) is thanked for the strontium isotope analysis. A. Comelli and H.
680 Nijs are kindly thanked for the careful preparation of the wafers and thin sections. L. Barchi is
681 gratefully appreciated for his help in SEM analysis. We gratefully acknowledge A. Koopman for
682 the constructive discussions during field work.
683

Solid Earth Discuss., https://doi.org/10.5194/se-2018-136
Manuscript under review for journal Solid Earth
Discussion started: 3 January 2019
© Author(s) 2019. CC BY 4.0 License.



## References

Alvarez, W.: Evolution of the Monte Nerone Seamount in the Umbria-Marches Apennines; I, Jurassic-Tertiary stratigraphy, B. Soc. Geol. Ital., 108, 3-21, 1989.

Amieux, P.: La cathodoluminescence: méthode d'étude sédimentologique des carbonates, B. Cent. Rech. Explor.-Prod. Elf-Aquitaine, 6, 437-483, 1982.

Artoni, A.: Messinian events within the tectono-stratigraphic evolution of the Southern Laga Basin (Central Apennines, Italy), B. Soc Geol. Ital., 122, 447-466, 2003.

Artoni, A.: The Pliocene-Pleistocene stratigraphic and tectonic evolution of the central sector of the Western Periadriatic Basin of Italy, Mar. Pet. Geol., 42, 82-106, https://doi.org/10.1016/j.marpetgeo.2012.10.005, 2013.

Banner, J. L.: Radiogenic isotopes: systematics and applications to earth surface processes and chemical stratigraphy, Earth. Sci. Rev., 65, 141-194, https://doi.org/10.1016/S0012-8252(03)00086-2, 2004.

Barchi, M., Minelli, G., and Pialli G.: The CROP 03 profile: a synthesis of results of deep structures of the Northern Apennines, Mem. Soc. Geol. It., 52, 383-400, 1998.

Barker, S. L., and Cox, S. F.: Evolution of fluid chemistry and fluid-flow pathways during folding and faulting: an example from Taemas, NSW, Australia, Geol. Soc. London Spec. Publ., 359, 203-227, https://doi.org/10.1144/SP359.12, 2011.

Bassetti, M. A., Ricci Lucchi, F., Roveri, M., Taviani, M.: Messinian facies in a critical section of northern Apennines (Montepetra-Perticara, Pesaro), Giorn. Geol., 60, 261-263, 1998.

Bathurst, R. G. C. (Eds.): Carbonate sediments and their diagenesis, Dev. Sedimentol., Ser., Elsevier, 12, 658 pp., 1975.

Bathurst, R. G. C.: Deep crustal diagenesis in limestones: Revista del Instituto de Investigaciones Geologicas, Deputacion Provincial, Universidad Barcelona, 34, 89-100, 1980.

Bernoulli, D., Kälin, O., and Patacca, E.: A sunken continental margin of the Mesozoic Tethys: The Northern and Central Apennines, Symposium" Sédimentation jurassique W Européen", Spec. Publ. Ass. Sedim. Francis, 1, 179-210, 1979.

Bodnar, R. J.: Revised equation and table for determining the freezing point depression of $H_2O$-NaCl solutions, Geochim. Cosmochim. Acta, 57, 683-684, 10.1016/0016-7037(93)90378-A, 1993.

© Author(s) 2019. CC BY 4.0 License.

715 Boles, J. R. and Franks, S. G.: Clay diagenesis in Wilcox Sandstone of southwest Texas:
716 Implications of smectite diagenesis and sandstone cementation, J. Sediment. Petrol.,
717 49, 55-70, https://doi.org/10.1306/212F76BC-2B24-11D7-8648000102C1865D,
718 1979.
719 Bollati, A., Corrado, S., and Marino, M.: Inheritance of Jurassic rifted margin architecture into
720 the Apennines Neogene mountain building: a case history from the Lucretili Mts.
721 (Latium, Central Italy), Int. J. Earth Sci., 101, 1011-1031,
722 https://doi.org/10.1007/s00531-011-0694-7, 2012.
723 Bosence, D., Procter, E., Aurell, M., Kahla, A. B., Boudagher-Fadel, M., Casaglia, F., Cirilli, S.,
724 Mehdie, M., Nieto, L., Rey, J., Scherreiks, R., Soussi, M., and Waltham, D.: A
725 dominant tectonic signal in high-frequency, peritidal carbonate cycles? A regional
726 analysis of Liassic platforms from western Tethys, J. Sediment. Res., 79, 389-415,
727 https://doi.org/10.2110/jsr.2009.038, 2009.
728 Boschetti, T., Venturelli, G., Toscani, L., Barbieri, M., and Mucchino, C.: The Bagni di Lucca
729 thermal waters (Tuscany, Italy): an example of $CaSO_4$ waters with high Na/Cl and
730 low $Ca/SO_4$ ratios, J. Hydrol., 307, 270-293,
731 https://doi.org/10.1016/j.jhydrol.2004.10.015, 2005.
732 Brandano, M., Cornacchia, I., Raffi, I., and Tomassetti, L.: The Oligocene-Miocene stratigraphic
733 evolution of the Majella carbonate platform (Central Apennines, Italy), Sediment.
734 Geol., 333, 1-14, https://doi.org/10.1016/j.sedgeo.2015.12.002, 2016.
735 Burke, W. H., Denison, R. E., Hetherington, E. A., Koepnick, R. B., Nelson, H. F., and Otto, J.
736 B.: Variation of seawater $^{87}Sr/^{86}Sr$ throughout Phanerozoic time, Geology, 10, 516-
737 519, https://doi.org/10.1130/0091-7613(1982)10<516:VOSSTP>2.0.CO;2, 1982.
738 Burkhard, M.: Calcite twins, their geometry, appearance and significance as stress-strain markers
739 and indicators of tectonic regime: a review, J. Struct. Geol., 15, 351-368,
740 https://doi.org/10.1016/0191-8141(93)90132-T, 1993.
741 Calamita, F., Cello, G., Deiana, G., and Paltrinieri, W.: Structural styles, chronology rates of
742 deformation, and time-space relationships in the Umbria-Marche thrust system
743 (central Apennines, Italy), Tectonics, 13, 873-881,
744 https://doi.org/10.1029/94TC00276, 1994.

© Author(s) 2019. CC BY 4.0 License.

745 Cardello, G. L., and Doglioni, C.: From mesozoic rifting to Apennine orogeny: the gran Sasso
746 range (Italy), Gondwana Res., 27, 1307-1334,
747 https://doi.org/10.1016/j.gr.2014.09.009, 2015.
748 Carpenter, B.: Origin and chemical evolution of brines in sedimentary basins, Oklahoma Geol.
749 Surv., 79, 60-77, https://doi.org/10.2118/7504-MS, 1978.
750 Centamore, E., Chiocchini, U., and Moretti, A.. Geologia della zona tra Acerenza e Avigliano
751 (Prov. di Potenza), Studi Geol. Camerti, 1, 97-122,
752 http://dx.doi.org/10.15165/studgeocam-1462, 1971.
753 Chilovi, C., De Feyter, A. J., Minelli, G., and Barchi, M. R.. Neogene strike-slip reactivation of
754 Jurassic normal faults in the M. Nerone-M. Catria Anticline (Umbro-Marchean Apennines,
755 Italy), Boll. Soc. Geol. It., 121, 199-207, 2002.
756 Choukroune, P., Gapais, D., and Merle, O.: Shear criteria and structural symmetry, J. Struct.
757 Geol., 9, 525-530, https://doi.org/10.1016/0191-8141(87)90137-4, 1987.
758 Clemenzi, L., Storti, F., Balsamo, F., Molli, G., Ellam, R., Muchez, P., and Swennen, R.: Fluid
759 pressure cycles, variations in permeability, and weakening mechanisms along low-
760 angle normal faults: The Tellaro detachment, Italy, Am. Assoc. Pet. Geol. Bull., 127,
761 1689-1710, https://doi.org/10.1130/B31203.1, 2015.
762 Colacicchi, R., Passeri, L., and Pialli, G.: Evidences of tidal environment deposition in the
763 Calcare Massiccio formation (Central Apennines-Lower Lias), in: Tidal Deposits,
764 edited by: Ginsburg, R. N., Springer, Berlin, Heidelberg, Germany, 345-353,
765 https://doi.org/10.1007/978-3-642-88494-8, 1975.
766 Cooper, J. C., and Burbi, L.: The geology of the central Sibillini Mountains, Mem. Soc. Geol. It.,
767 35, 323-347, 1986.
768 Crescenti, U.: Serie stratigrafiche della serie calcarea dal Lias al Miocene nella regione
769 Marchigiano Abruzzese: parte I and II, Mem. Soc. Geol. It., 8, 155-420, 1969.
770 Davies, G. R., and Smith, L. B. J.: Structurally controlled hydrothermal dolomite reservoir
771 facies: an overview, Am. Assoc. Pet. Geol. Bull., 90, 1641-1690, 2006.
772 Del Moro, A., Puxeddu, M., Radicati di Brozolo, F., and Villa, I. M.: Rb-Sr and K-Ar ages of
773 minerals at temperatures of 300-400°C from deep wells in the Larderello geothermal
774 field (Italy), Contrib. Mineral. Petr., 81, 349-349,
775 https://doi.org/10.1007/BF00371688, 1982.

© Author(s) 2019. CC BY 4.0 License.

776 Dewever, B., Swennen, R., and Breesch, L.: Fluid flow compartmentalization in the Sicilian fold
777 and thrust belt: implications for the regional aqueous fluid flow and oil migration
778 history, Tectonophysics, 591, 194-209, https://doi.org/10.1016/j.tecto.2011.08.009,
779 2013.
780 Dewey, J. F., Helman, M. L., Turco, E., Hutton, D. H. W., and Knott, S. D.: Kinematics of the
781 western Mediterranean, in: Alpine Tectonics, edited by: Coward, M. P., Dietrich, D.,
782 Park, R. G., Geol. Soc. London Spec. Publ., 45, 265-283,
783 https://doi.org/10.1144/GSL.SP.1989.045.01.15, 1989.
784 Dewit, J., Foubert, A., El Desouky, H. A., Muchez, P., Hunt, D., Vanhaecke, F., and Swennen,
785 R.: Characteristics, genesis and parameters controlling the development of a large
786 stratabound HTD body at Matienzo (Ramales Platform, Basque-Cantabrian Basin,
787 northern Spain), Mar. Pet. Geol., 55, 6-25, 10.1016/j.marpetgeo.2013.12.021, 2014.
788 Dickson, J. A. D.: Carbonate identification and genesis as revealed by staining, J. Sediment.
789 Petrol., 36, 491-505, https://doi.org/10.1306/74D714F6-2B21-11D7-
790 8648000102C1865D, 1966.
791 Di Francesco, L., Fabbi, S., Santantonio, M., Bigi, S., and Poblet, J.: Contribution of different
792 kinematic models and a complex Jurassic stratigraphy in the construction of a
793 forward model for the Montagna dei Fiori fault-related fold (Central Apennines,
794 Italy), Geol. J., 45, 489-505, https://doi.org/10.1002/gj.1191, 2010.
795 Elter, P., Giglia, G., Tongiorgi, M., and Trevisan, L.: Tensional and contractional areas in the
796 recent (Tortonian to Present) evolution of the Northern Apennines, B. Geofis. Teor.
797 Appl., 17, 3-18, 1975.
798 Emery, D., and Robinson, A. (Eds.): Inorganic Geochemistry: Applications to Petroleum
799 Geology, Blackwell Science, Oxford, United Kingdom, 101-128, 1993.
800 Fantoni, R., and Franciosi, R.: Tectono-sedimentary setting of the Po Plain and Adriatic foreland,
801 Rend. Lincei , 21, 197-209, https://doi.org/10.1007/s12210-010-0102-4, 2010.
802 Flecker, R., De Villiers, S., and Ellam, R. M.: Modelling the effect of evaporation on the
803 salinity-$^{87}Sr/^{86}Sr$ relationship in modern and ancient marginal-marine systems: the
804 Mediterranean Messinian Salinity Crisis, Earth Planet. Sci. Lett., 203, 221-233,
805 10.1016/S0012-821X(02)00848-8, 2002.

© Author(s) 2019. CC BY 4.0 License.

Friedman, I.: Some investigations of the deposition of travertine from Hot Springs-I. The isotopic chemistry of a travertine-depositing spring, Geochim. Cosmochim. Acta, 34, 1303-1315, https://doi.org/10.1016/0016-7037(70)90043-8, 1970.

Gale, J. F., Laubach, S. E., Marrett, R. A., Olson, J. E., Holder, J., and Reed, R. M.: Predicting and characterizing fractures in dolostone reservoirs: Using the link between diagenesis and fracturing, Geol. Soc. London Spec. Publ., 235, 177-192, https://doi.org/10.1144/GSL.SP.2004.235.01.08, 2004.

Giacometti, A., and Ronchi, P.: Early Lias Carbonate Platform: Facies and Diagenesis Analogies between the Calcare Massiccio (Umbro-Marchean Apennines) and the Inici Fm. (Sicily Channel), Mem. Soc. Geol. It., 55, 271-278, 2000.

Ghisetti, F., and Vezzani, L.: Detachments and normal faulting in the Marche fold-and-thrust belt (Central Apennines, Italy): inferences on fluid migration paths, J. Geodyn., 29, 345-369, https://doi.org/10.1016/S0264-3707(99)00057-5, 2000.

Ghisetti, F., and Vezzani, L.: Interfering paths of deformation and development of arcs in the fold-and-thrust belt of the central Apennines (Italy), Tectonics, 16, 523-536, https://doi.org/10.1029/97TC00117, 1997.

Goldstein, R. H., and Reynolds, T. J.: Systematics of Fluid Inclusions in Diagenetic Minerals, Soc. Sediment. Geol., Short Course, 31, 199 pp., 1994.

Gregg, J. M.: On the formation and occurrence of saddle dolomite-discussion, J. Sediment. Petrol., 53, 1025-1033, 1983.

Gregg, J. M., Shelton, K. L., Johnson, A. W., Somerville, I. D., and Wright, W. R.: Dolomitization of the Waulsortian limestone (lower Carboniferous) in the Irish Midlands, Sedimentology, 48, 745-766, https://doi.org/10.1046/j.1365-3091.2001.00397.x, 2001.

Habermann, D., Neuser, R. D., and Richter, D. K.: REE-activated cathodoluminescence of calcite and dolomite: high-resolution spectrometric analysis of CL emission (HRS-CL), Sediment. Geol., 101, 1-7, https://doi.org/10.1016/0037-0738(95)00086-0, 1996.

Hendry, J. P., Gregg, J. M., Shelton, K. L., Somerville, I. D., and Crowley, S. F.: Origin, characteristics and distribution of fault-related and fracture-related dolomitization:

© Author(s) 2019. CC BY 4.0 License.

Insights from Mississippian carbonates, Isle of Man, Sedimentology, 62, 717-752, https://doi.org/10.1111/sed.12160, 2015.

Hiemstra, E. J., and Goldstein, R. H.: Repeated injection of hydrothermal fluids into downdip carbonates: a diagenetic and stratigraphic mechanism for localization of reservoir porosity, Indian Basin Field, New Mexico, USA, Geol. Soc. London Spec. Publ., 406, 141-177, https://doi.org/10.1144/SP406.1, 2015.

Horita, J.: Oxygen and carbon isotope fractionation in the system dolomite-water-$CO_2$ to elevated temperatures, Geochim. Cosmochim. Acta, 129, 111-124, https://doi.org/10.1016/j.gca.2013.12.027, 2014.

Horvath, F.: Towards a mechanical model for the formation of the Pannonian basin, Tectonophysics, 226, 333-357, https://doi.org/10.1016/0040-1951(93)90126-5, 1993.

Hudson, J. D.: Stable isotopes and limestone lithification, Geol. Soc. London, 133, 637-660, https://doi.org/10.1144/gsjgs.133.6.0637, 1977.

Koopman, A.: Detachment tectonics in the central Apennines, Italy, Ph.D. thesis, Utrecht University, The Netherlands, 155 pp., 1983.

Land L. S.: The isotopic and trace element geochemistry of dolomite: the state of the art, in: Concepts and Models of dolomitization, edited by: Zenger D. H., Dunham J. B. and Ethington R. L., Soc. Econ. Paleontol. and Mineral., Spec. Pub., 28, 87-110, 1980.

Land L. S.: The application of stable isotopes to studies of the origin of dolomite and to problems of diagenesis of clastic sediments, in: Stable Isotopes in Sedimentary Geology, edited by: Arthur M. A., Soc. Econ. Paleontol. and Mineral, Short Course, 10, 4-1 , 1983.

Land L. S.: The origin of massive dolomite. Jour. Geol. Educ., 33, 112-125, 1985.

Laubach, S. E., Eichhubl, P., Hilgers, C., and Lander, R. H.: Structural diagenesis, J. Struct. Geol., 32, 1866-1872, https://doi.org/10.1016/j.jsg.2010.10.001, 2010.

Li, Z., Goldstein, R. H. and Franseen, E. K.: Meteoric calcite cementation: diagenetic response to relative fall in sea-level and effect on porosity and permeability, Las Negras area, southeastern Spain, Sediment. Geol., 348, 1-18, https://doi.org/10.1016/j.sedgeo.2016.12.002, 2017.

© Author(s) 2019. CC BY 4.0 License.

Lind, I. L., Berger, W. H., and Kroenke, L. W.: Stylolites in chalk from leg 130, Ontong Java Plateau, in: Proceedings of the Ocean Drilling Program, scientific results, 445-451, 1993.

Lobato, L. M., Forman, J. M. A., Fazikawa, K., Fyfe, W. S., and Kerrich, R.: Uranium in overthrust Archean basement, Bahia, Brazil. Canadian Mineral., 21, 647-654, 1983.

Luczaj, J. A., and Goldstein, R. H.: Diagenesis of the Lower Permian Krider Member, southwest Kansas, USA: fluid-inclusion, U-Pb, and fission-track evidence for reflux dolomitization during latest Permian time, J. Sediment. Res., 70, 762-773, https://doi.org/10.1306/2DC40936-0E47-11D7-8643000102C1865D, 2000.

Machel, H. G.: Effects of groundwater flow on mineral diagenesis, with emphasis on carbonate aquifers, Hydrol. J., 7, 94-107, https://doi.org/10.1007/s100400050, 1999.

Machel, H. G., Mason, R. A., Mariano, A. N., and Mucci, A.: Causes and emission of luminescence in calcite and dolomite, in: Luminescence microscopy and spectroscopy : Qualitative and quantitative applications, edited by: Barker, C. E., and Kopp, O. C, Soc. Sediment. Geol., Short Course, 9-25, 1991.

Machel, H. G., and Cavell, P. A.: Low-flux, tectonically-induced squeegee fluid flow, Bull. Can. Petrol. Geol., 47, 510-533, 1999.

Major, R. P., Lloyd, R. M. and Lucia, F. J.: Oxygen isotope composition of Holocene dolomite formed in a humid hypersaline setting, Geology, 20, 586-588, https://doi.org/10.1130/0091-7613(1992)020<0586:OICOHD>2.3.CO;2, 1992.

Marchegiani, L., Deiana, G., and Tondi, E.: Tettonica pre-orogenica in Appennino centrale, Stud. Geol. Camerti, 14, 211-228, http://dx.doi.org/10.15165/studgeocam-807, 1999.

Marino, M., and Santantonio, M.: Understanding the geological record of carbonate platform drowning across rifted Tethyan margins: Examples from the Lower Jurassic of the Apennines and Sicily (Italy), Sediment. Geol., 225, 116-137, https://doi.org/10.1016/j.sedgeo.2010.02.002, 2010.

Marshall, J. D.: Climatic and oceanographic isotopic signals from the carbonate rock record and their preservation, Geol. Mag., 129, 143-160, https://doi.org/10.1017/S0016756800008244, 1992.

Mattei, M.: Analisi geologico-strutturale della Montagna dei Fiori (Ascoli Piceno, Italia Centrale), Geol. Romana, 26, 327-347, 1987.

© Author(s) 2019. CC BY 4.0 License.

Mazzoli, S., Deiana, G., Galdenzi, S., and Cello, G.: Miocene fault-controlled sedimentation and thrust propagation in the previously faulted external zones of the Umbria-Marche Apennines, Italy, EGU Stephan Mueller Spec. Publ. Ser., 1, 195-209, 2002.

Mazzullo, S. J.: Geochemical and neomorphic alteration of dolomite: a review, Carbonates Evaporites, 7, 21-37, https://doi.org/10.1007/BF03175390, 1992.

McArthur, J. M., Howarth, R. J., and Shields, G. A.: Strontium isotope stratigraphy, in: The Geologic Time Scale 2012, edited by: Gradstein, F. M., Ogg, J. G., Schmitz, M., and Ogg, G., Elsevier, 127-144, https://doi.org/10.1016/C2011-1-08249-8, 2012.

McCaffrey, M. A., Lazar, B., Holland, H. D.: The evaporation path of seawater and the coprecipitation of Br- and Kþ with halite, J. Sediment. Res., 57, 928-937, https://doi.org/10.1306/212F8CAB-2B24-11D7-8648000102C1865D, 1987.

McCaig, A. M.: Deep fluid circulation in fault zones, Geology, 16, 867-870, https://doi.org/10.1130/0091-7613(1988)016<0867:DFCIFZ>2.3.CO;2, 1988.

McCaig, A. M., Wickham, S. M., and Taylor, H. P.: Deep fluid circulation in alpine shear zones, Pyrenees, France: field and oxygen isotope studies, Contrib. Mineral. Petr., 106, 41-60, https://doi.org/10.1007/BF00306407, 1990.

Montanez, I. P.: Late diagenetic dolomitization of Lower Ordovician, upper Knox carbonates: A record of the hydrodynamic evolution of the southern Appalachian Basin, Am. Assoc. Pet. Geol. Bull., 78, 1210-1239, 1994.

Moore, C. H. (Eds.): Carbonate diagenesis and porosity, Dev. Sedimentol., 46, Elsevier Sci. Publ., Amsterdam, The Netherlands, 338 pp., 1989.

Morettini, E., Santantonio, M., Bartolini, A., Cecca, F., Baumgartner, P. O., and Hunziker, J. C.: Carbon isotope stratigraphy and carbonate production during the Early-Middle Jurassic: examples from the Umbria-Marche-Sabina Apennines (central Italy), Paleog., Paleocl., Paleoec., 184, 251-273, https://doi.org/10.1016/S0031-0182(02)00258-4, 2002.

Mountjoy, E. W., Machel, H. G., Green, D., Duggan, J., and Williams-Jones, A. E.: Devonian matrix dolomites and deep burial carbonate cements: a comparison between the Rimbey-Meadowbrook reef trend and the deep basin of west-central Alberta, B. Can. Petrol. Geol., 47, 487-509, 1999.

© Author(s) 2019. CC BY 4.0 License.

926 Murgia, M. V., Ronchi, P., and Ceriani, A.: Dolomitization processes and their relationships with
927 the evolution of an orogenic belt (Central Apennines and peri-adriatic foreland,
928 Italy), AAPG Hedberg series, 1, 277-294, https://doi.org/10.1306/1025695H13121,
929 2004.
930 Nelson, R. A: Significance of fracture sets associated with stylolite zones, Am. Assoc. Pet. Geol.
931 Bull., 65, 2417-2425, 1981.
932 Parotto, M., and Praturlon, A.: Geological summary of the Central Apennines, Quad. Ric. Sci.,
933 90, 257-311, 1975.
934 Patacca, E., Sartori, R., and Scandone, P.: Tyrrhenian basin and Apenninic arcs: Kinematic
935 relations since late Tortonian times, Mem. Soc. Geol. It., 45, 425-451,
936 http://hdl.handle.net/11568/11610, 1992.
937 Pialli, G.: Facies di piana cotidale nel Calcare Massiccio dell'Appennino umbro marchigiano,
938 Boll. Soc. Geol. It., 90, 481-507, 1971.
939 Pierantoni, P., Deiana, G., and Galdenzi, S.: Stratigraphic and structural features of the Sibillini
940 Mountains (Umbria-Marche Apennines, Italy), Ital. J. Geosci., 132, 497-520,
941 https://doi.org/10.3301/IJG.2013.08, 2013.
942 Purser, B., Tucker, M. and Zenger, D.: Problems, progress and future research concerning
943 dolomites and dolomitization, in: Dolomites: a Volume in Honour of Dolomieu,
944 edited by: Purser, B., Tucker, M. and Zenger, D., IAS Spec. Publ., 21, 3-20, 1994.
945 Radke, B. M., and Mathis, R. L.: On the formation and occurrence of saddle dolomite, J.
946 Sediment. Res., 50, 1149-1168, https://doi.org/10.1306/212F7B9E-2B24-11D7-
947 8648000102C1865D, 1980.
948 Ronchi, P., Casaglia, F., and Ceriani, A.: The multiphase dolomitization of the Liassic Calcare
949 Massiccio and Corniola successions (Montagna dei Fiori, Northern Apennines, Italy),
950 Boll. Soc. Geol. It., 122, 157-172, 2003.
951 Rosenbaum, J., and Sheppard, S. M.: An isotopic study of siderites, dolomites, and ankerites at
952 high temperatures, Geochim. Cosmochim. Acta, 50, 1147-1150,
953 https://doi.org/10.1016/0016-7037(86)90396-0, 1986.
954 Roveri, M., Bassetti, M. A., and Lucchi, F. R.: The Mediterranean Messinian salinity crisis: an
955 Apennine foredeep perspective, Sediment. Geol., 140, 201-214,
956 https://doi.org/10.1016/S0037-0738(00)00183-4, 2001.

© Author(s) 2019. CC BY 4.0 License.

957 Saelen, G., Doyle, P., and Talbot, M. R.: Stable-isotope analyses of belemnite rostra from the
958 Whitby Mudstone Fm., England: Surface water conditions during deposition of a
959 marine black shale, Palaios, 11, 97-117, https://doi.org/10.2307/3515065, 1996.
960 Santantonio, M, and Carminati, E.: Jurassic rifting evolution of the Apennines and Southern Alps
961 (Italy): Parallels and differences, Geol. Soc. Am. B., 123, 464-484,
962 https://doi.org/10.1130/B30104.1, 2011.
963 Santantonio, M. and Muraro, C.: The Sabina Plateau, Palaeoescrapment, and Basin-Central
964 Apennines, 6th international symposium on the Jurassic system, General Field Trip
965 Guidebook, Palermo, Italy, 271-315, 2002.
966 Santantonio, M., Fabbi, S., and Bigi, S.: Discussion on «Geological map of the partially
967 dolomitized Jurassic succession exposed in the central sector of the Montagna dei
968 Fiori Anticline, Central Apennines, Italy», Ital. J. Geosci., 136, 312-316,
969 https://doi.org/10.3301/IJG.2017.04, 2017.
970 Schulz, H. M., Wirth, R., and Schreiber, A.: Organic-inorganic rock-fluid interactions in
971 stylolitic micro-environments of carbonate rocks: a FIB-TEM study combined with a
972 hydrogeochemical modelling approach, Geofluids, 16, 909-924,
973 https://doi.org/10.1111/gfl.12195, 2016.
974 Scisciani V., Tavarnelli, E., and Calamita, F.: The interaction of extensional and contractional
975 deformations in the outer zones of the Central Apennines, Italy, J. Struct. Geol., 24,
976 1647-1658, https://doi.org/10.1016/S0191-8141(01)00164-X, 2002.
977 Shackleton, N. J., and Kennett, J. P.: Paleotemperature History of the Cenozoic and the Initiation
978 of Antartic Glaciation Oxygen and Carbon Isotope Analyses in DSDP Sites 277, 279,
979 and 281, Initial reports of Deep Sea Drilling Project, 29, 743-755, 1975.
980 Sharp, I., Gillespie, P., Morsalnezhad, D., Taberner, C., Karpuz, R., Vergés, J., Horbury, A.,
981 Pickard, N., J. Garland, J., and Hunt, D.: Stratigraphic architecture and fracture-
982 controlled dolomitization of the Cretaceous Khami and Bangestan groups: an outcrop
983 case study, Zagros Mountains, Iran, Geol. Soc. London Spec. Publ., 329, 343-396,
984 https://doi.org/10.1144/SP329.14, 2010.
985 Shepherd, T., Rankin, A. H., and Alderton, D. H. M. (Eds.): A Practical Guide to Fluid Inclusion
986 Studies, Glasgow: Blackie, 239 pp., 1985.

© Author(s) 2019. CC BY 4.0 License.

Sibley, D. F., and Gregg, J. M.: Classification of dolomite rock textures, J. Sediment. Petrol., 57, 967-975, https://doi.org/10.1306/212F8CBA-2B24-11D7-8648000102C1865D, 1987.

Sibson, R. H.: Fluid flow accompanying faulting: field evidence and models, Earthquake prediction: an international review, AGU, 4, 593-603, https://doi.org/10.1029/ME004p0593, 1981.

Slobodník, M., Muchez, P., Kral, J., and Keppens, E.: Variscan veins: record of fluid circulation and Variscan tectonothermal events in Upper Palaeozoic limestones of the Moravian Karst, Czech Republic, Geol. Mag., 143, 491-508, https://doi.org/10.1017/S0016756806001981, 2006.

Smith, R. E., Wiltschko, D. V.: Generation and maintenance of abnormal fluid pressures beneath a ramping thrust sheet: isotropic permeability experiments, J. Struct. Geol., 18, 951-970, https://doi.org/10.1016/0191-8141(96)00023-5, 1996.

Steiger, R., and Jäger, E.: Subcommission on geochronology: convention on the use of decay constants in geo and cosmochronology, Earth Planet. Sci. Lett., 36, 359-362, https://doi.org/10.1016/0012-821X(77)90060-7, 1977.

Storti, F., Balsamo, F., and Koopman, A.: Geological map of the partially dolomitized Jurassic succession exposed in the core of the Montagna dei Fiori Anticline, Central Apennines, Italy, Ital. J. Geosci., 136, 125-135, https://doi.org/10.3301/IJG.2016.05, 2017a.

Storti F., Balsamo, F., and Koopman, A.: Reply to: discussion on «Geological map of the partially dolomitized Jurassic succession exposed in the central sector of the Montagna dei Fiori Anticline, Central Apennines, Italy» by Santantonio, M., Fabbi, S. and Bigi, S., Ital. J. Geosci., 136, 317-319, https://doi.org/10.3301/IJG.2017.04, 2017b.

Storti, F., Balsamo F., Mozafari M., Koopman A., Swennen R. and Taberner C.: Syn-contractional overprinting between extension and shortening along the Montagna dei Fiori Fault during Plio-Pleistocene antiformal stacking at the Central Apennines thrust wedge toe, Tectonics, https://doi.org/10.1029/2018TC005072, 2018.

© Author(s) 2019. CC BY 4.0 License.

Stueber, A. M., Pushkar, P., and Baldwin, A. D., JR.: Survey of $^{87}Sr/^{86}Sr$ ratios and total strontium concentrations in Ohio stream and ground waters, Ohio J. Sci., 72, 98-104, 1972.

Sommer, S. E.: Cathodoluminescence of carbonates, 1. Characterization of cathodoluminescence from carbonate solid solutions, Chemical Geology, 9, 257-273, https://doi.org/10.1016/0009-2541(72)90064-2, 1972.

Swennen, R., Dewit, J., Fierens, E., Muchez, Ph., Shah, M., Nader, F. H., Hunt, D.: Multiple dolomitisation events along the Ranero fault (Pozalagua Quarry, BasqueeCantabrian Basin): episodic earthquake activity, Sedimentology, 59, 1345-1374, https://doi.org/10.1111/j.1365-3091.2011.01309.x, 2012.

Tavani, S., Storti, F., Salvini, F., and Toscano, C.: Stratigraphic versus structural control on the deformation pattern associated with the evolution of the Mt. Catria anticline, Italy, J. Struct. Geol., 30, 664-681, https://doi.org/10.1016/j.jsg.2008.01.011, 2008.

Taylor, H. P.: Oxygen and hydrogen isotope relationships in hydrothermal mineral deposits, In: Geochemistry of hydrothermal ore deposits, edited by: Barnes, H. L., Wiley and Sons, New york, 229-302, 1997.

Thirlwall, M. F.: Long-term reproducibility of multicollector Sr and Nd isotope ratio analysis, Chemical Geology, 94, 85-104, https://doi.org/10.1016/S0009-2541(10)80021-X, 1991.

Tongiorgi, M., Rau, A., and Martini, I. P.: Sedimentology of early-alpine, fluvio-marine, clastic deposits (Verrucano, Triassic) in the Monti Pisani (Italy), Sediment. Geol., 17, 311-332, https://doi.org/10.1016/0037-0738(77)90051-3, 1977.

Vai, G. B., and Ricci Lucchi, F.: Algal crusts, autochthonous and clastic gypsum in a cannibalistic evaporite basin: a case history from the Messinian of northern Apennines. Sedimentology, 24, 221-244, https://doi.org/10.1111/j.1365-3091.1977.tb00255.x, 1977.

Vandeginste, V., Swennen, R., Gleeson, S. A., Ellam, R. M., Osadetz, K., and Roure, F.: Zebra dolomitization as a result of focused fluid flow in the Rocky Mountains Fold and Thrust Belt, Canada. Sedimentology, 52, 1067-1095, https://doi.org/10.1111/j.1365-3091.2005.00724.x, 2005.

© Author(s) 2019. CC BY 4.0 License.

1046 Vandeginste, V., Swennen, R., Gleeson, S. A., Ellam, R. M., Osadetz, K., and Roure, F.:
1047 Geochemical constraints on the origin of the Kicking Horse and Monarch Mississippi
1048 Valley-type lead-zinc ore deposits, southeast British Columbia, Canada, Mineralium
1049 Deposita, 42, 913-935, https://doi.org/10.1007/s00126-007-0142-6, 2007.
1050 Veizer, J., Ala, D., Azmy, K., Bruckshen, P., Buhl, D., Bruhn, F., Carden, G. A. F., Diener, A.,
1051 Ebneth, S., Godderis, Y., Jasper, T., Korte, C., Pawellek, F., Podlaha, O. G., and
1052 Strauss, H.: $^{87}Sr/^{86}Sr$, $\delta^{13}C$ and evolution of Phanerozoic seawater, Chemical
1053 Geology, 161, 59-88, https://doi.org/10.1016/S0009-2541(99)00081-9, 1999.
1054 Walker, G., Abumere, O. E., and Kamaluddin, B.: Luminescence spectroscopy of Mn2 rock-
1055 forming carbonates, Mineral. Mag., 53, 201-11, 10.1180/minmag.1989.053.370.07,
1056 1989.
1057 Wilson, A., and Ruppel, C.: Salt tectonics and shallow subseafloor fluid convection: models of
1058 coupled fluid-heat-salt transport, Geofluids, 7, 377-386,
1059 https://doi.org/10.1111/j.1468-8123.2007.00191.x, 2007.
1060 Woodcock, N. H., and Mort, K.: Classification of fault breccias and related fault rocks, Geol.
1061 Mag., 145, 435-440, https://doi.org/10.1017/S0016756808004883, 2008.
1062 Zempolich, W. G., and Hardie, L. A.: Geometry of dolomite bodies within deep-water
1063 resedimented oolite of the Middle Jurassic Vajont Limestone, Venetian Alps, Italy:
1064 Analogs for hydrocarbon reservoirs created through fault-related burial
1065 dolomitization, in: Reservoir quality prediction in sandstones and carbonates, edited
1066 by: Kupecz, A., Gluyas, J., and Bloch, S., AAPG Mem., 69, 127-162, 1997.

1067

1068

1069

1070

1071

1072

Solid Earth Discuss., https://doi.org/10.5194/se-2018-136
Manuscript under review for journal Solid Earth
Discussion started: 3 January 2019
© Author(s) 2019. CC BY 4.0 License.



**Table captions**

**Table. 1**. Stable carbon and oxygen isotopes, $^{87}Sr/^{86}Sr$ ratios, and fluid inclusion microthermometry data (not pressure corrected) of host rocks and diagenetic phases in the Montagna dei Fiori Anticline. Stable carbon and oxygen isotopes values are expressed in ‰ V-PDB and salinity values in eq. wt. % NaCl.

**Figure captions**

Fig. 1. A) Simplified regional map (modified after Ghisetti and Vezzani, 1997) showing the tectonic outlines of the Central Apennines and the study area (rectangle). B) Schematic geological map of the Montagna dei Fiori Anticline showing the distribution of dolostones (modified after Storti et al., 2017a). C) Lithostratigraphical column of the successions exposed in Montagna dei Fiori (modified after Mattei, 1987; Di Francesco et al, 2010; Storti et al., 2018). Lithologies are mentioned in the text. Note that the thickness of the not-outcropping formations (Triassic evaporites and the crystalline basement) is not to scale. D) Geological transect across present day Central Apennines and the Adriatic Sea (modified after Fantoni and Franciosi, 2010) with vertical exaggeration of 2:1. The dashed rectangle indicates the Montagna dei Fiori Anticline region.

Fig. 2. A, B) Geological map of the central sector of the Montagna dei Fiori Anticline, and cross-section oriented parallel (a-b) to the hinge line representing the tectono-stratigraphic architecture of the faulted anticline (modified after Storti et al., 2017a). The stereonets (Schmidt equal area projection lower hemisphere) provide the attitude of the extensional faults. The locations of the corresponding field sites are indicated by numbers.

Fig. 3. A) Field photograph showing the deformed Scaglia Formation in the hanging wall (HW) and brecciated, dolomitized Calcare Massiccio Formation in the footwall (FW) of the Montagna dei Fiori Fault. B) A hand specimen from the deformed Scaglia formation showing the intensity of the pressure solutions (TS) and their abutting relationship with calcite veins (CV2). C) A transmitted light photomicrograph of the dolomitized, brecciated Calcare Massiccio Formation. Note all the breccia fragments are composed of dolomite (D4 here).

© Author(s) 2019. CC BY 4.0 License.

Fig. 4. Field photographs (Corano Quarry) showing the field relations between dolostones, host limestones and the Montagna dei Fiori Fault: A) Panoramic view showing the spatial relationship between limestones and dolostones (orange) in the damage zone of the Montagna dei Fiori Fault (F). Note that the limestones and including dolostones of the Calcare Massiccio and Bugarone Formations on the footwall (FW) and marly limestones of the Scaglia Formation on the hangingwall (HW) are intensely deformed. B) Plan view of the Calcare Massiccio limestone in the footwall damage zone: intersected by calcite veins (CV1), dolomitized and affected by bed perpendicular stylolites (arrows). C) Distinct transition (dashed line) between dolomitized and undolomitized Calcare Massiccio limestone in the footwall damage zone.

Fig. 5. Field photograph (A) and a simplified sketch (B) of a dolomitic pocket within the folded Calcare Massiccio (grey color) and their relation with bed parallel stylolites (hammer is 40 cm long).

Fig. 6. A) Transmitted light image showing a micritic peloid rimmed by the fibrous cements (FC) which are followed by the mosaic cements (MC). B) Transmitted light image showing mosaic cements (MC) in a peloidal limestone over printed by high amplitude bed parallel stylolites (dotted white line). Note the core of some of the peloids is partially cemented as well. C, D) Respectively, transmitted light and corresponding cathodoluminescence image of FC and MC cements. E) Transmitted light photomicrograph showing D1 crystals rimming a fracture which is cemented by CV1. The fracture is in turn affected by a bed parallel stylolite. F) Cathodoluminescence image showing D1 scattered in the host rock and riming the fracture. G, H) Respectively, transmitted light and corresponding cathodoluminescence image showing part of a bed parallel stylolite (dotted white line) overprinting D1 and D2 crystals.

Fig. 7. A, B) Photomicrographs of respectively, transmitted light and corresponding cathodoluminescence image showing the zoned rhombs of D2 with the remnants of D1 preserved in their cloudy core. The pore space is occluded by D4. C, D) D3 cementing angular breccia fragments of the Bugarone Formation in the damage zone of the Montagna dei Fiori Fault in the Corano Quarry site. Note the breccia is overprinted by a fault parallel bed perpendicular stylolite. E, F) Photomicrographs of respectively, transmitted light and corresponding

© Author(s) 2019. CC BY 4.0 License.

cathodoluminescence image showing the euhedral to subhedral crystals of D3 developing a bright subzone and rim. G, H) D3 with a saddle crystal outline (SD) postdating calcite cements (MC) and a zoned D2 crystal. The saddle morphology is outlined by a dotted white line.

Fig. 8. Photomicrographs of respectively, transmitted light and corresponding cathodoluminescence image of dolomite types: A, B) The cross-cutting relationship between D3 and D4. Note the presence of D3 within the core of dolomite crystals overgrown by D4. C, D) Successions of dolomite types. Note the green CL color of D4 crystals. Typically, luminescent dolomites are known to show yellow, orange to red colors (Machel et al., 1991). Green luminescence in carbonates including dolomite have been attributed by a number of researchers to the incorporation of three valent rare earth elements (REE) such as $Dy^{3+}$ and $U^{3+}$ as luminescence activators within their crystal lattice (Luczaj and Goldstein, 2000). Another possibility is the emplacement of $Mn^{2+}$, with yellow luminescence, in $Ca^{2+}$ sites with blue luminescence in the dolomite crystal lattice instead of preferential incorporation in the $Mg^{2+}$ site (Sommer, 1972b; Amieux, 1982; Walker et al., 1989; Habermann et al., 1999). Accordingly, non-stoichiometric, Ca-rich and poorly ordered dolomites may favor $Mn^{+2}$ incorporation into their $Ca^{2+}$ site. E, F) Vuggy porosity rimmed by D4 (green CL). Note the porosity is filled with fine dolomite rhombs including traces of D2 in their core and D4 overgrowths.

Fig. 9. Photomicrographs showing respectively, transmitted light and corresponding cathodoluminescence image of D4 and D5 in relation to stylolites and fracturing: A, B) D4, exploiting a bed parallel stylolite that crossed-cuts D1 and D2. C, D) A sub-horizontal fracture cemented by D4. E, F) D5 microveins (arrows) intersecting all the predating dolomite types in the footwall brecciated zone of the Montagna dei Fiori Fault.

Fig. 10. Field photographs showing the major calcite vein settings observed in Montagna dei Fiori: A) Cross-sectional view of bed normal Calcite vein 1 (CV1) abutting bed parallel stylolites in folded beds of the Calcare Massiccio Formation. B) Plan view of the Calcite vein 2 (CV2) intensely affecting the deformed Scaglia (Rossa) Formation. C, D) Cross-sectional view of the Scaglia Formation, intensely affected by pressure solution seams of tectonic origin crossed-over by populations of bed-perpendicular Calcite veins (CV3) in en echelon extensional arrays.

Solid Earth Discuss., https://doi.org/10.5194/se-2018-136
Manuscript under review for journal Solid Earth
Discussion started: 3 January 2019
© Author(s) 2019. CC BY 4.0 License.



Fig. 11. A) Cathodoluminescence and transmitted light (in set) image showing blocky to elongated crystals of CV1 with zoned CL pattern. B) Transmitted light image showing intensely twinned CV1 crystals overprinted by euhedral to subhedral crystals of D3. Photomicrographs of respectively, transmitted light and corresponding cathodoluminescence image: C, D) CV2 in the Scaglia Formation abutted by a bed perpendicular stylolite (indicated by white arrows and dashed line). The crystals display blocky to fibrous morphologies, deformation twining, and a similar orange luminescence pattern comparable with the adjacent host rock. E, F) CV3 cementing the breccia fragments in the damage zone of the Montagna dei Fiori Fault. The crystals are blocky and show faint deformation twinning. They are brown-orange with distinct darker luminescence sector zones. G, H) CV4 present as a cement within a polygonal pore space rimmed by dolomite. Note the blocky crystals, absence of deformation twinning and distinct concentric luminescence zonation pattern. CV4 is corroded and followed by a late telogenetic calcite.

Fig. 12. A , B) Overview of the $\delta^{13}C$ and $\delta^{18}O$ values of dolomites (A) host rocks from Montagna dei Fiori as well as calcite veins (B). The stable isotope value of Lower Jurassic marine limestones based on Veizer et al. (1999) is indicated by a dashed rectangle in subset B. The $\delta^{18}O$ values of the marine dolomites are considered to be 3-4‰ V-PDB higher than those of marine limestones (Land, 1980; Major et al., 1992; Horita, 2014). C) Cross-plot of $^{87}Sr/^{86}Sr$ ratios and corresponding $\delta^{18}O$ values of host rocks, dolomites and calcite veins compared with Lower Jurassic marine carbonates $^{87}Sr/^{86}Sr$ (dashed rectangle) framework reported by McArthur et al. (2012).

Fig. 13. Overview of microthermometry analysis of primary inclusions in Montagna dei Fiori: A) Frequency distribution of the $Tm_{ice}$ (°C) in dolomite phases. B) Frequency distribution of the Th (°C) in dolomite phases. C) Salinity (eq. wt. % NaCl) versus Th (°C) of dolomite and calcite phases. D) Isotopic fractionation diagram from Land (1983) used to determine the isotopic composition (‰ V-SMOW) of parental fluids in equilibrium with dolomites in Montagna dei Fiori.

Solid Earth Discuss., https://doi.org/10.5194/se-2018-136
Manuscript under review for journal Solid Earth
Discussion started: 3 January 2019
© Author(s) 2019. CC BY 4.0 License.



1196 Fig. 14. A) Generalized paragenesis of diagenetic phases in relation to deformational stages and
1197 burial history of the Calcare Massiccio Formation in the Montagna dei Fiori Anticline. The
1198 deformational stages are from Storti et al. (2018), and the burial curve is based on Ronchi et al.
1199 (2003).
1200
1201 Fig. 15. Sketch showing the successive fault-related diagenetic phases, of most importantly
1202 dolomitization, recorded in the carbonate succession exposed at the core of the Montagna dei
1203 Fiori Anticline (not scaled). Different diagenetic phases are indicated with different colors. A)
1204 The first dolomitization event is pre-orogenic (syn-rift), triggered from the fluids channelized
1205 along Jurassic extensional faults. This event occurred during burial compaction and development
1206 of bed parallel stylolites (BS). It is represented by scattered dolomite rhombs (D1) followed by
1207 calcite cementation (CV1). The dolomitization continued with precipitation of larger crystals of
1208 D2. B) Second dolomitization event: syn-orogenic (early folding/ faulting) dolomitization from
1209 fluids that migrated from more internal regions of the thrust belt and were channelized along the
1210 basal detachment level into the fold core. This dolomitization event presents matrix replacive and
1211 cements displaying infrequent saddle outlines (SD) in pore spaces, within bed parallel veins and
1212 shear fractures. These dolostones postdate compaction but are affected by bed perpendicular
1213 stylolites (TS) generated by horizontal to sub-horizontal layer parallel shortening related to the
1214 growth of the Montagna dei Fiori Anticline. C) Extensional collapse of the anticline and
1215 development of the Montagna dei Fiori Fault, followed by buttressing of the Scaglia against
1216 Calcare Massiccio and Corniola Formations during positive inversion induced by continuing
1217 underthrusting at depth. Precipitation of D5 in micro-veins and cements in breccia zones,
1218 followed by late stage calcite cementation in the Montagna dei Fiori Fault damage zone (CV2,
1219 CV3 and CV4).

Solid Earth Discuss., https://doi.org/10.5194/se-2018-136
Manuscript under review for journal Solid Earth
Discussion started: 3 January 2019
© Author(s) 2019. CC BY 4.0 License.

| | Stable isotopes | | Sr isotopes | Fluid inclusion microthermometry | |
|---|---|---|---|---|---|
| | $\delta^{13}C$ | $\delta^{18}O$ | $^{87}Sr/^{86}Sr$ | Th (°C) | Salinity |
| Calcare Massiccio Fm. | +2.4 to +3.1 | -1.6 to 0.0 | 0.70766 | - | - |
| Corniola Fm. | +2.0 to +2.5 | -3.1 to -1.4 | 0.70725 | - | - |
| Scaglia Fm. | +1.0 to +3.1 | -2.2 to -1.0 | 0.70784-0.70791 | - | - |
| D1 | +2.5 | -1.9 | 0.70789 | ≤ 40-50 | 3.5 to 11.3 |
| CV1 | +1.6 to +2.1 | -4.7 to -2.7 | 0.70773 | - | - |
| D2 | - | - | - | ≤ 40-50 to 71 | 7.9 to 20.5 |
| D3 | +2.0 to +2.6 | -2.8 to -1.9 | 0.70859-0.70964 | 70 to 73 | 9.2 to 16.9 |
| D4 | +2.4 to +2.5 | -3.0 to -2.5 | 0.70790 | 79 to 105 | 12.8 to 18.6 |
| CV2 | +1.2 to +3.1 | -1.7 to -1.6 | 0.70779 - 0.70787 | - | - |
| CV3 | +0.5 to +2.4 | -2.2 to 0.0 | - | ≤ 40-50 | 4.5 to 9.7 |
| CV4 | +3.8 to +4.9 | -9.4 to -9.1 | - | ≤ 40-50 | 0.17 to 3.0 |

Table. 1

Solid Earth Discuss., https://doi.org/10.5194/se-2018-136
Manuscript under review for journal Solid Earth
Discussion started: 3 January 2019
© Author(s) 2019. CC BY 4.0 License.

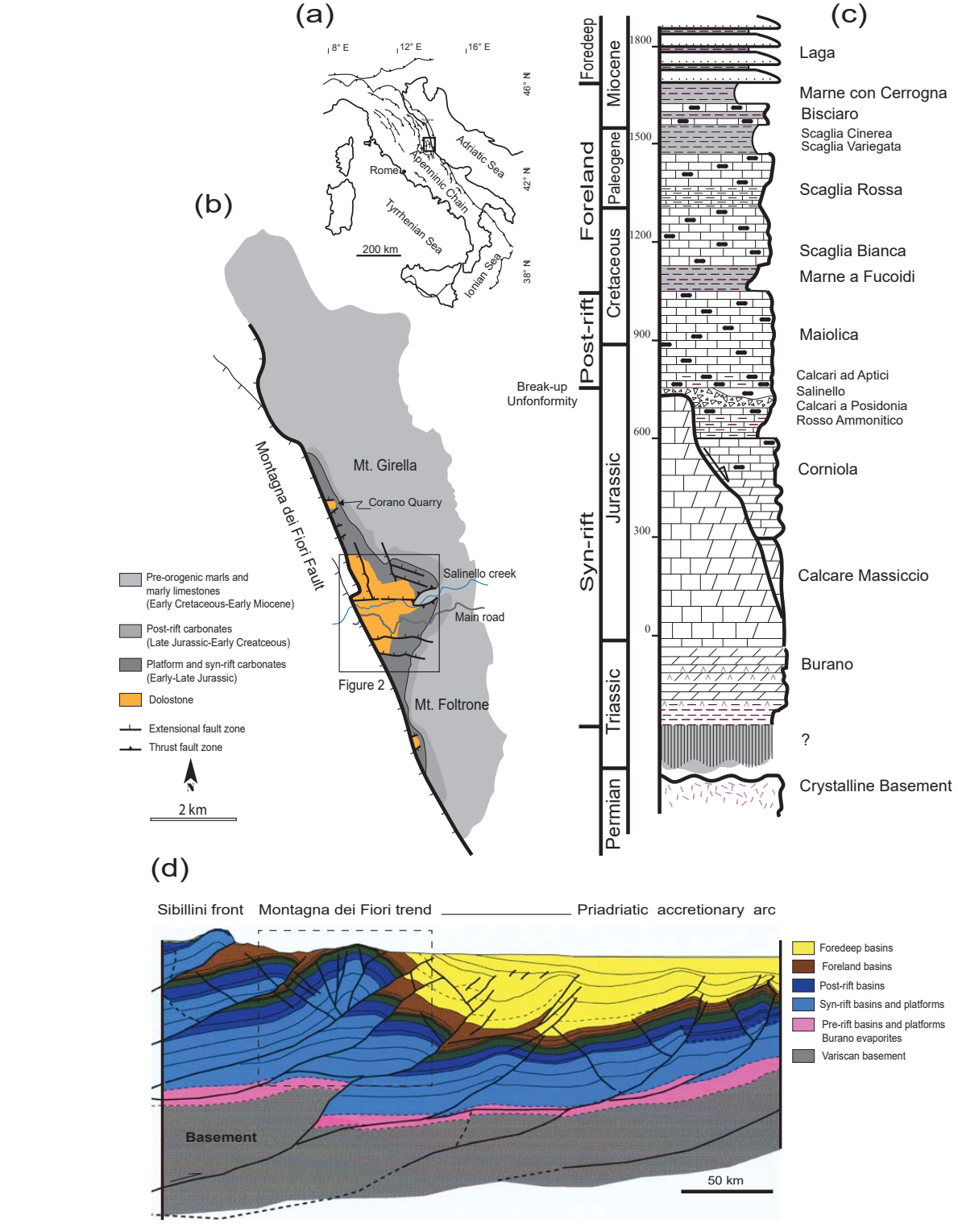


Fig. 1

Solid Earth Discuss., https://doi.org/10.5194/se-2018-136
Manuscript under review for journal Solid Earth
Discussion started: 3 January 2019
© Author(s) 2019. CC BY 4.0 License.

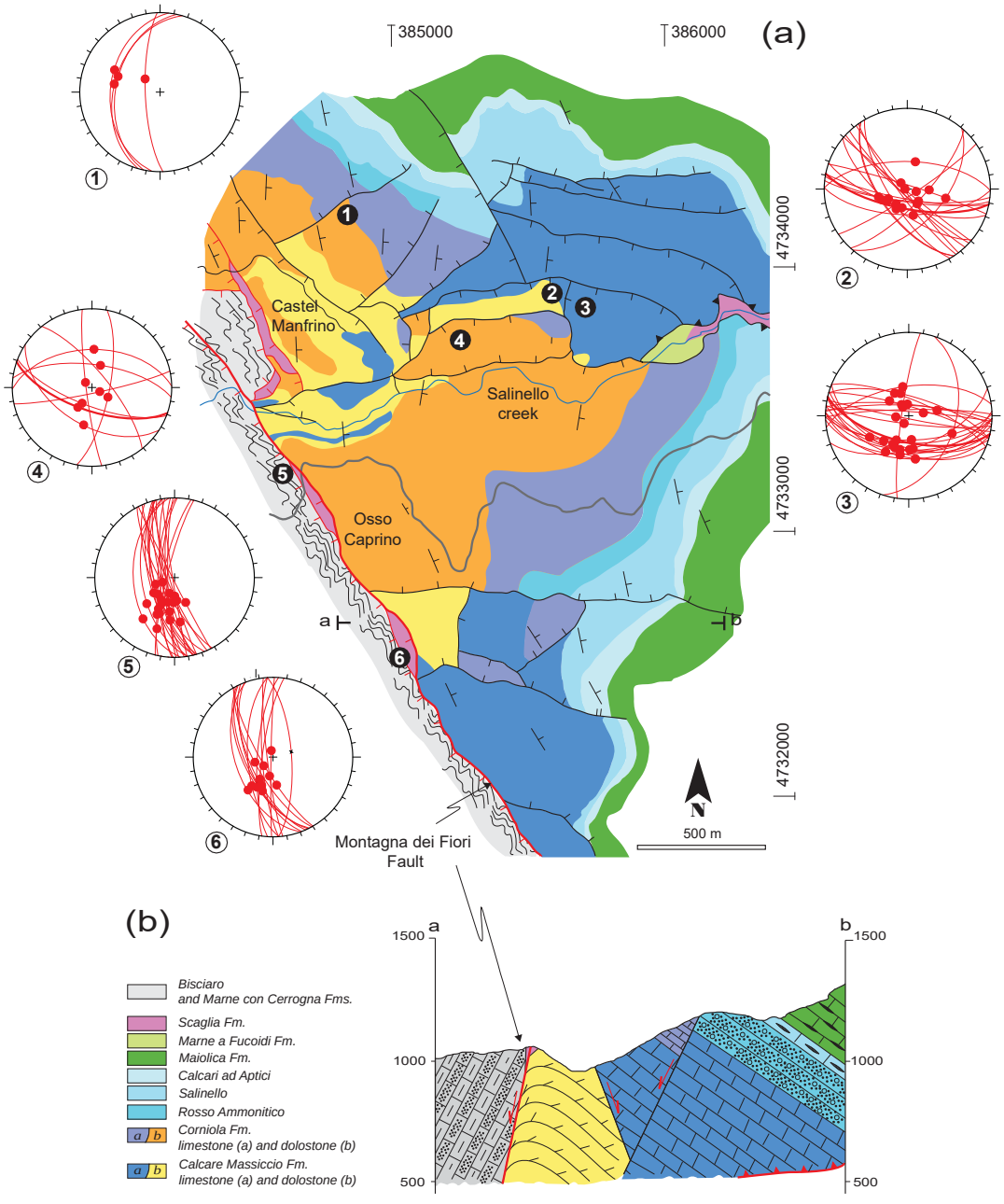


Fig. 2

Solid Earth Discuss., https://doi.org/10.5194/se-2018-136
Manuscript under review for journal Solid Earth
Discussion started: 3 January 2019
© Author(s) 2019. CC BY 4.0 License.

Solid Earth
Discussions
Open Access
EGU

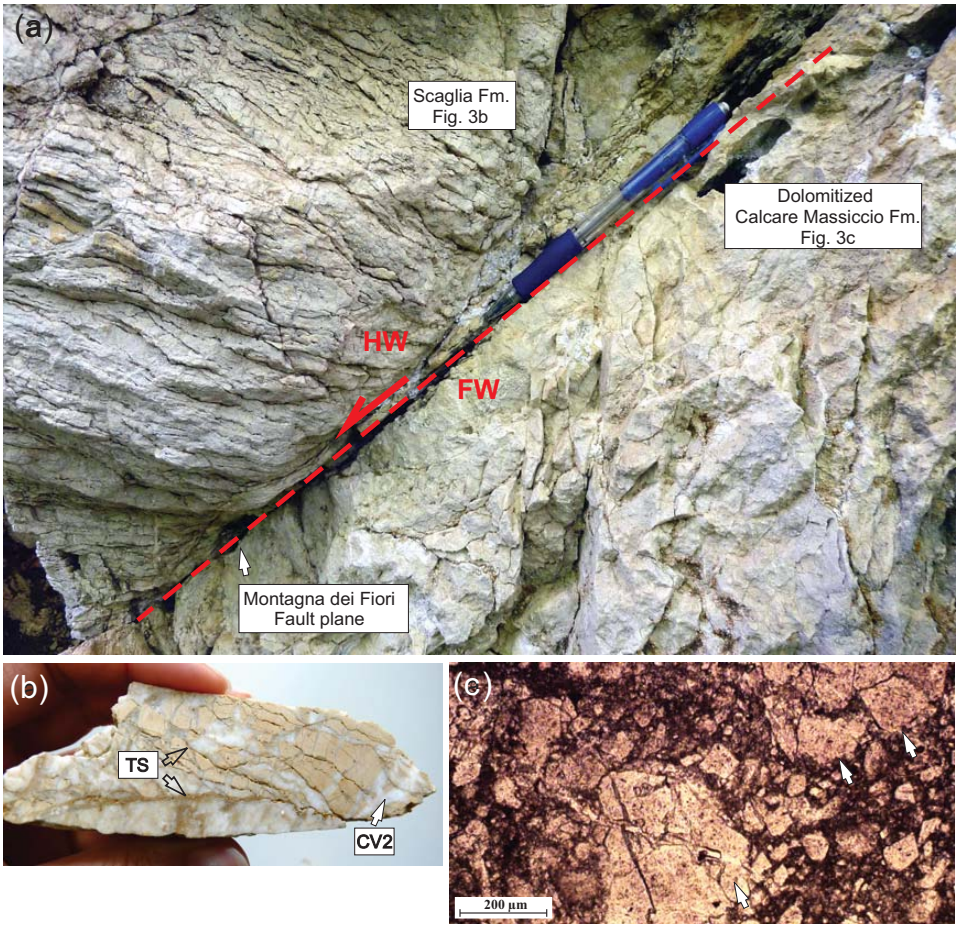


Fig. 3

Solid Earth Discuss., https://doi.org/10.5194/se-2018-136
Manuscript under review for journal Solid Earth
Discussion started: 3 January 2019
© Author(s) 2019. CC BY 4.0 License.

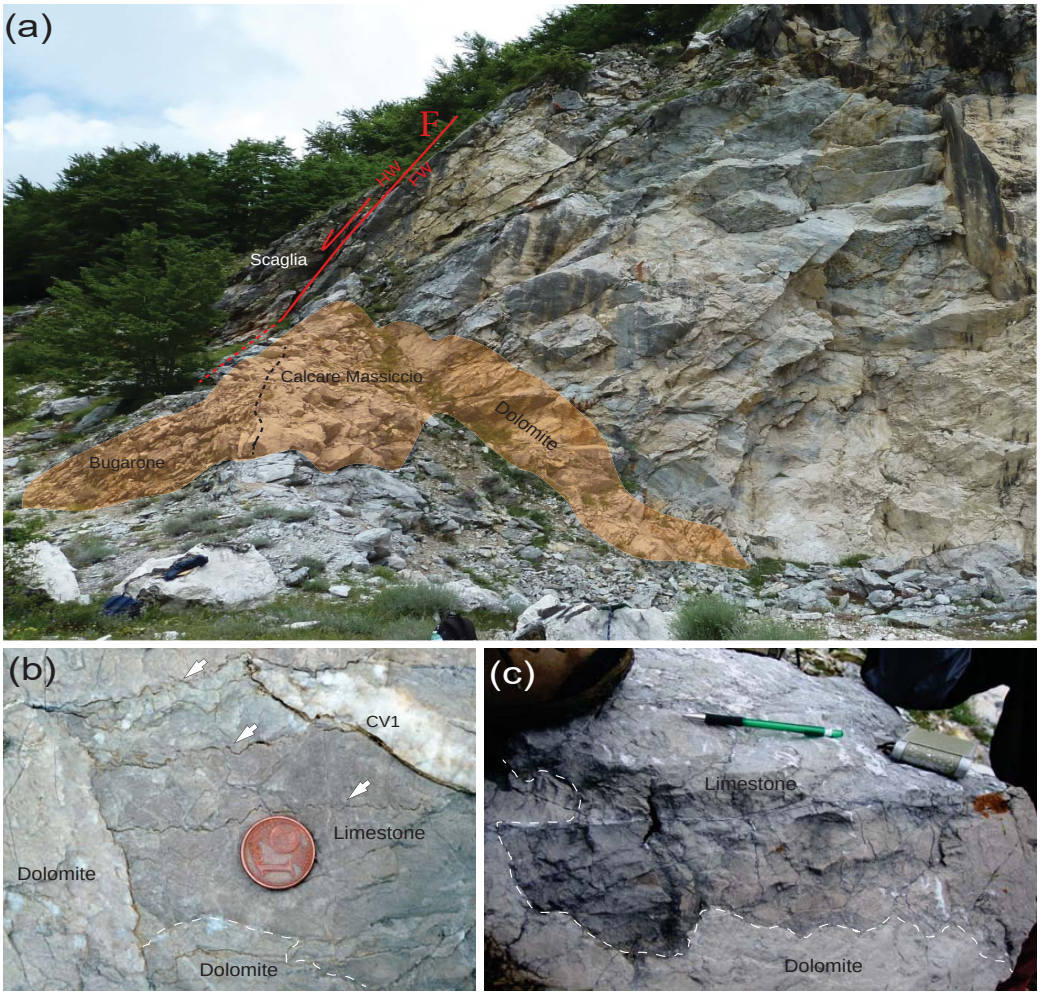


Fig. 4

Solid Earth Discuss., https://doi.org/10.5194/se-2018-136
Manuscript under review for journal Solid Earth
Discussion started: 3 January 2019
© Author(s) 2019. CC BY 4.0 License.

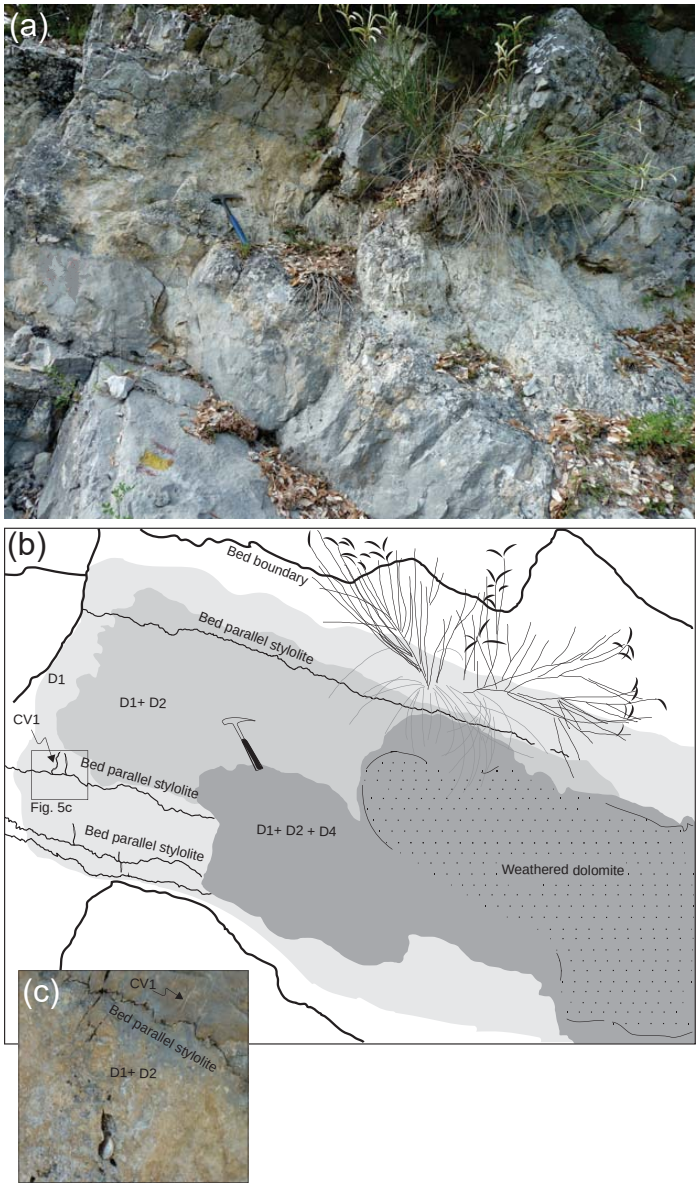


Fig. 5

Solid Earth Discuss., https://doi.org/10.5194/se-2018-136
Manuscript under review for journal Solid Earth
Discussion started: 3 January 2019
© Author(s) 2019. CC BY 4.0 License.

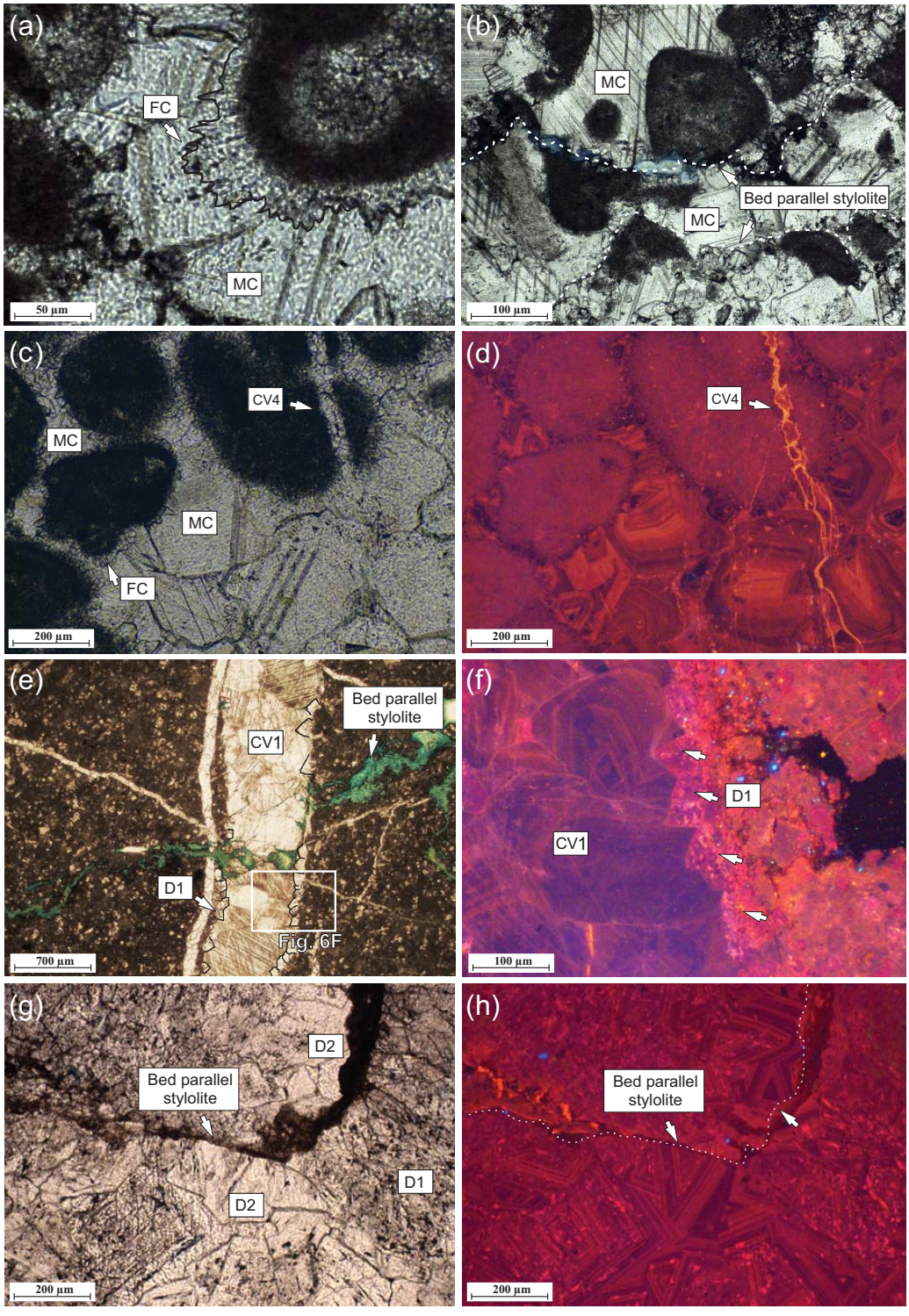


Fig 6

Solid Earth Discuss., https://doi.org/10.5194/se-2018-136
Manuscript under review for journal Solid Earth
Discussion started: 3 January 2019
© Author(s) 2019. CC BY 4.0 License.

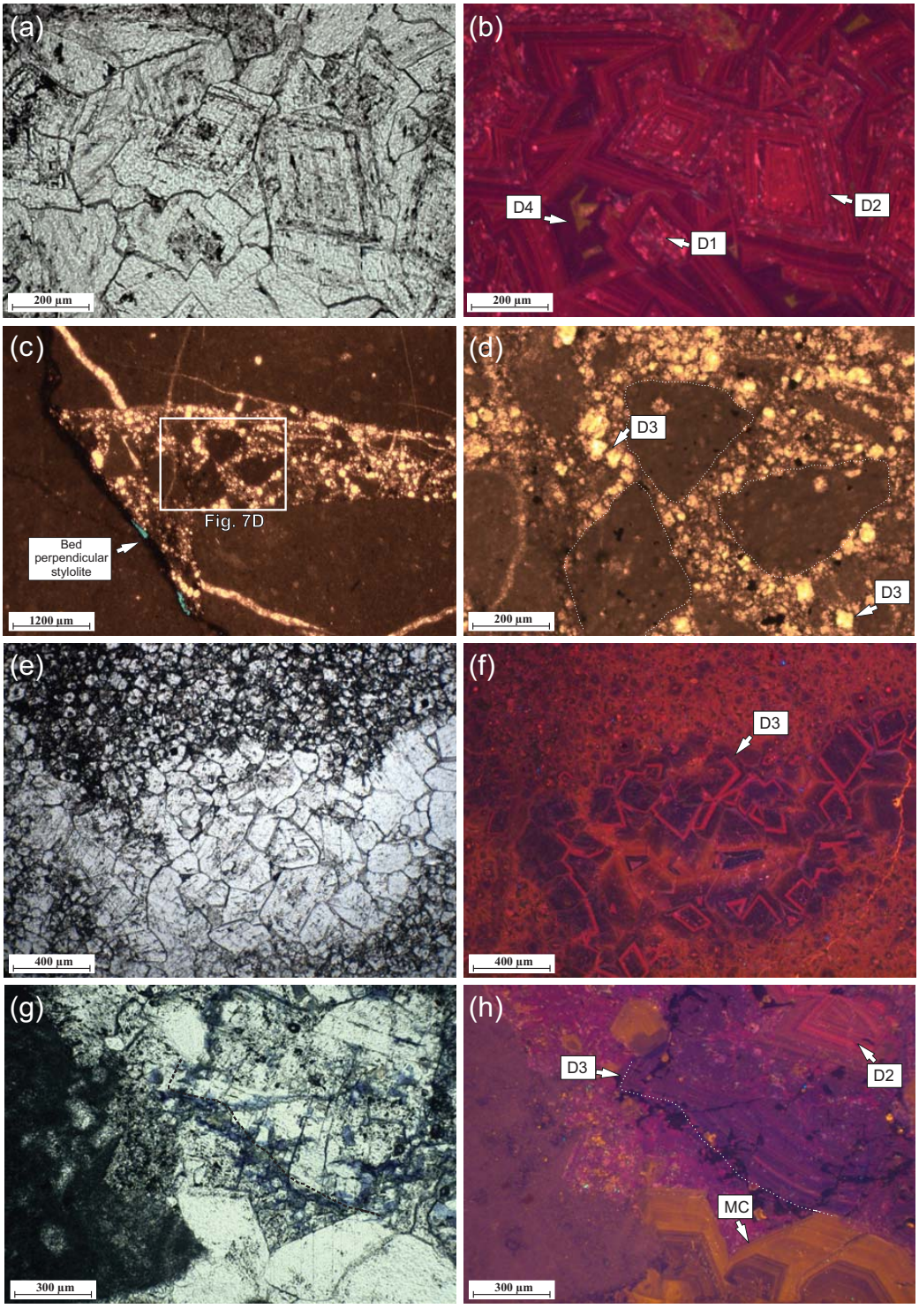


Fig. 7

Solid Earth Discuss., https://doi.org/10.5194/se-2018-136
Manuscript under review for journal Solid Earth
Discussion started: 3 January 2019
© Author(s) 2019. CC BY 4.0 License.

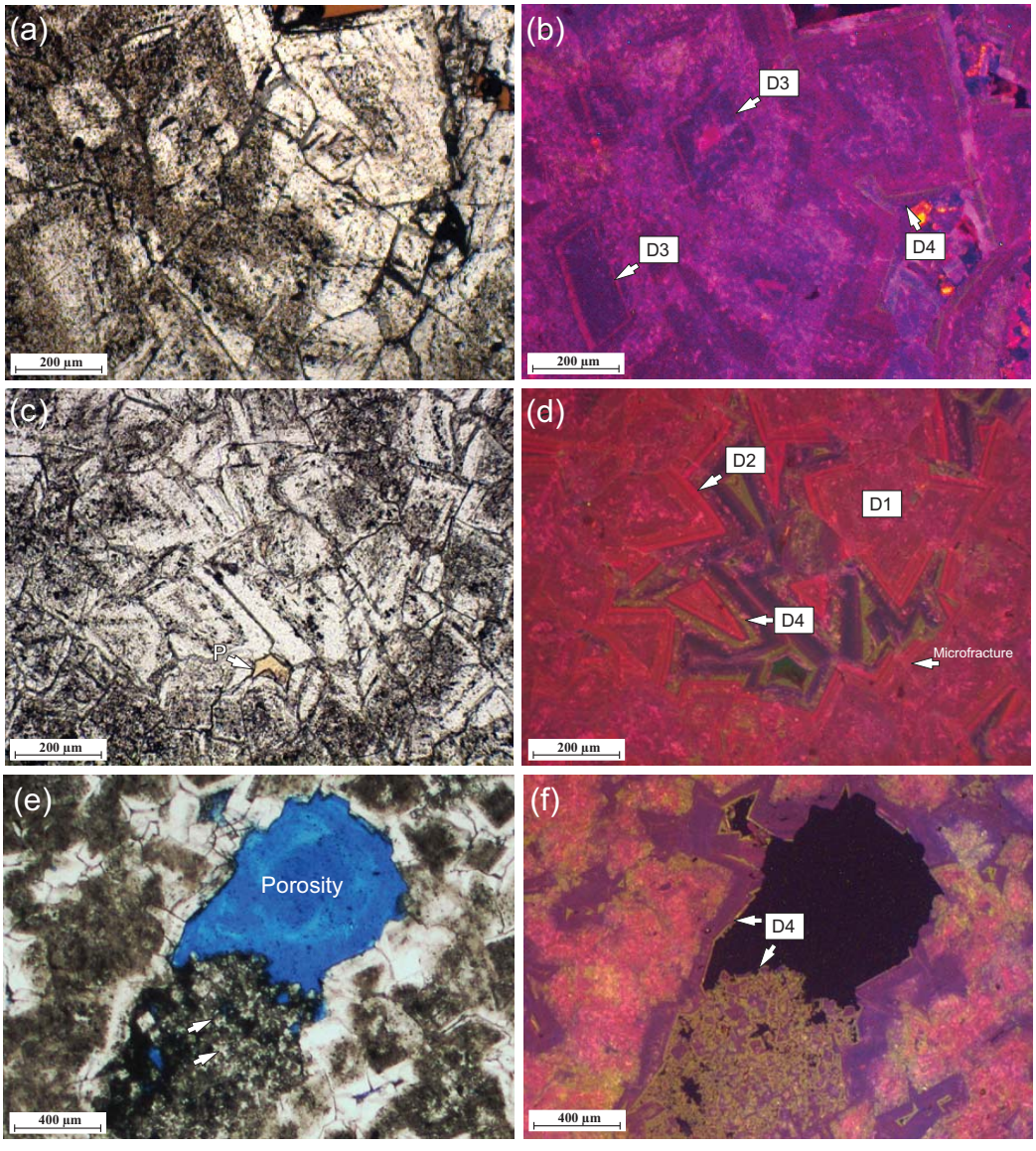


Fig. 8

Solid Earth Discuss., https://doi.org/10.5194/se-2018-136
Manuscript under review for journal Solid Earth
Discussion started: 3 January 2019
© Author(s) 2019. CC BY 4.0 License.

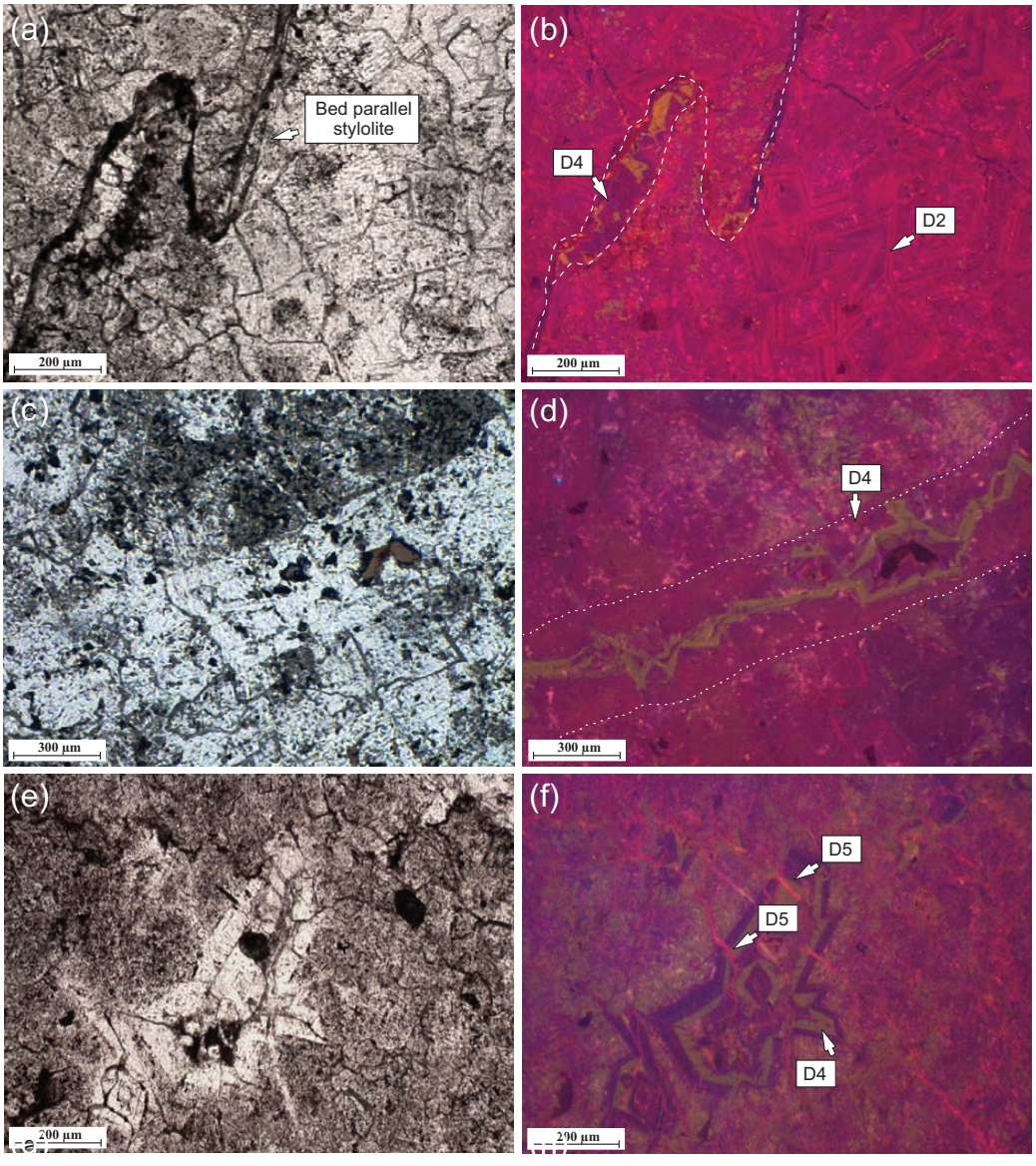


Fig. 9

Solid Earth Discuss., https://doi.org/10.5194/se-2018-136
Manuscript under review for journal Solid Earth
Discussion started: 3 January 2019
© Author(s) 2019. CC BY 4.0 License.

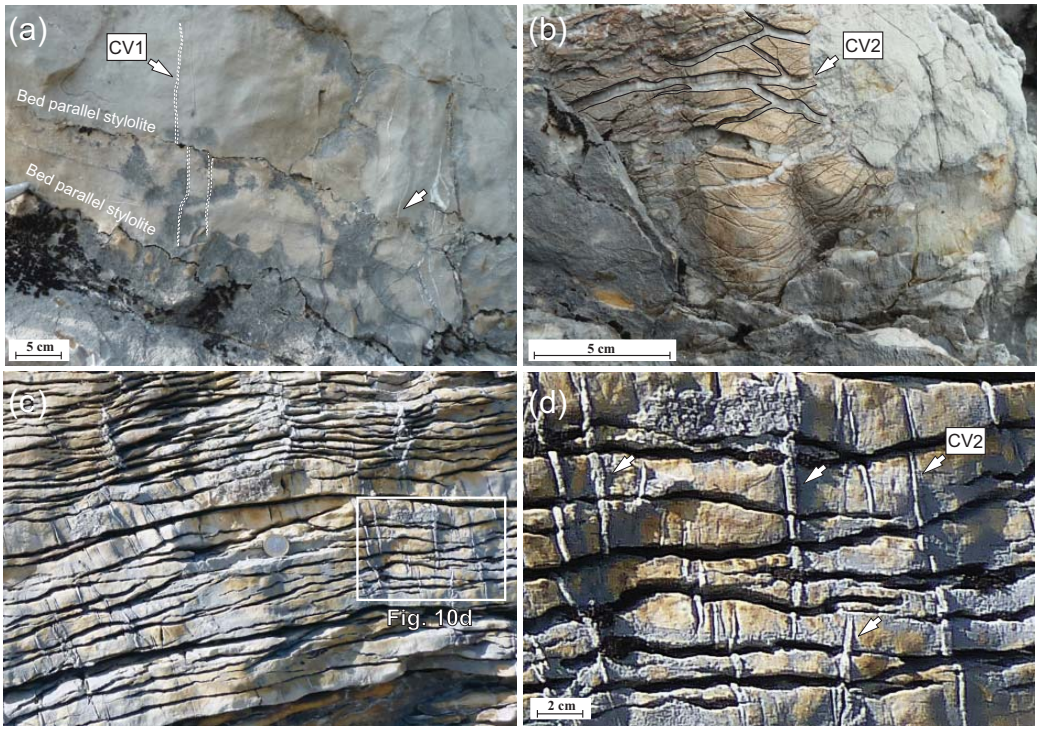


Fig. 10

Solid Earth Discuss., https://doi.org/10.5194/se-2018-136
Manuscript under review for journal Solid Earth
Discussion started: 3 January 2019
© Author(s) 2019. CC BY 4.0 License.

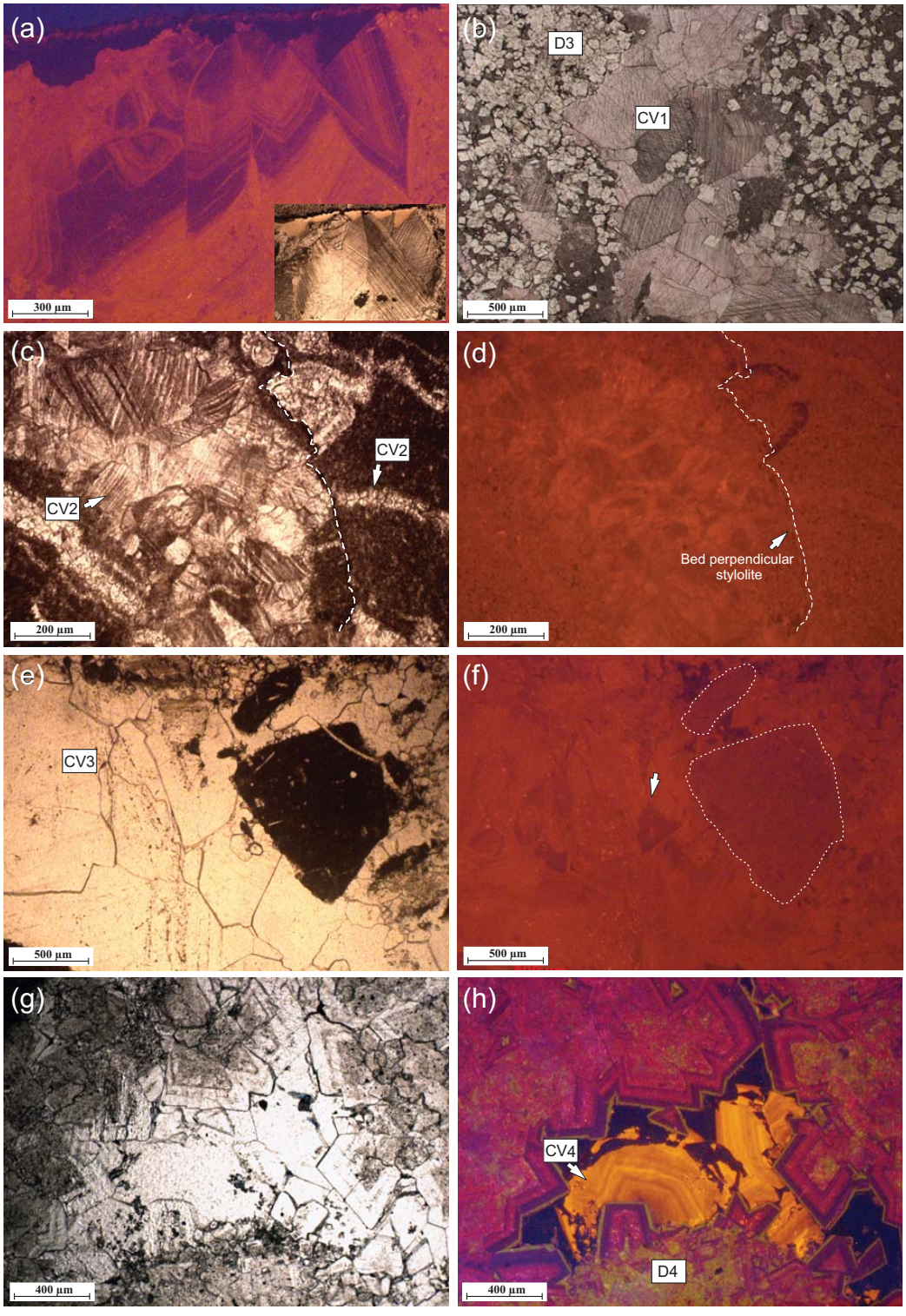


Fig. 11

Solid Earth Discuss., https://doi.org/10.5194/se-2018-136
Manuscript under review for journal Solid Earth
Discussion started: 3 January 2019
© Author(s) 2019. CC BY 4.0 License.

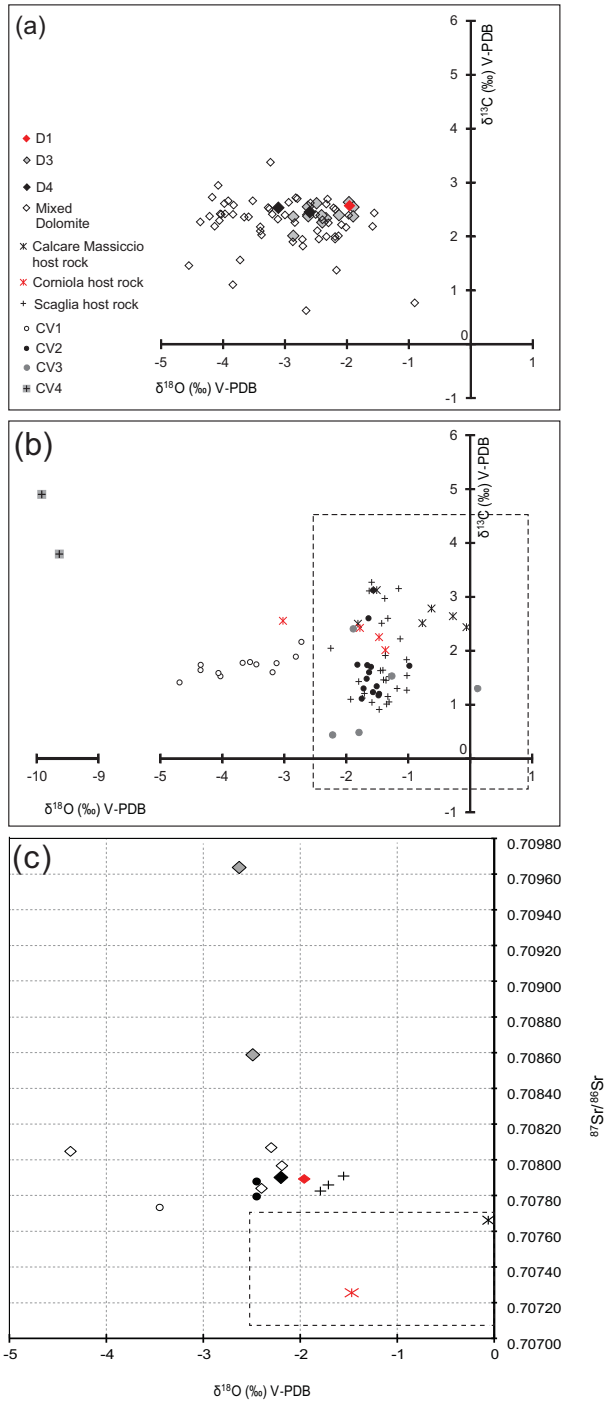


Fig. 12

Solid Earth Discuss., https://doi.org/10.5194/se-2018-136
Manuscript under review for journal Solid Earth
Discussion started: 3 January 2019
© Author(s) 2019. CC BY 4.0 License.

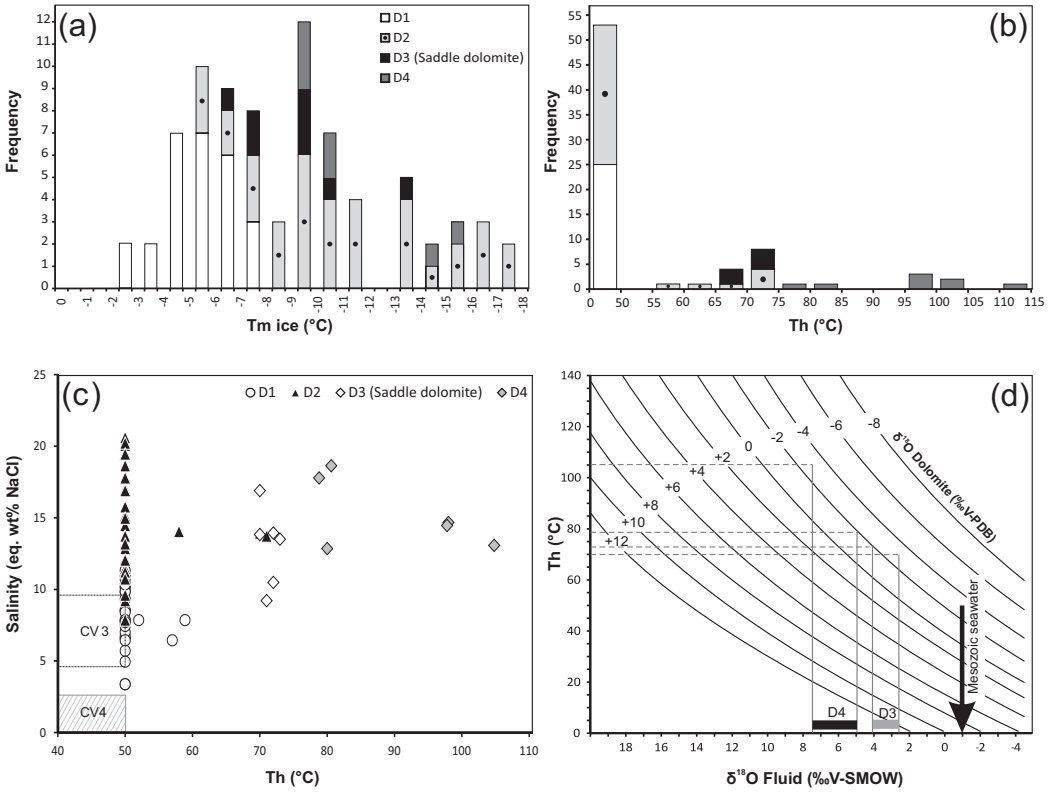


Fig. 13

Solid Earth Discuss., https://doi.org/10.5194/se-2018-136
Manuscript under review for journal Solid Earth
Discussion started: 3 January 2019
© Author(s) 2019. CC BY 4.0 License.

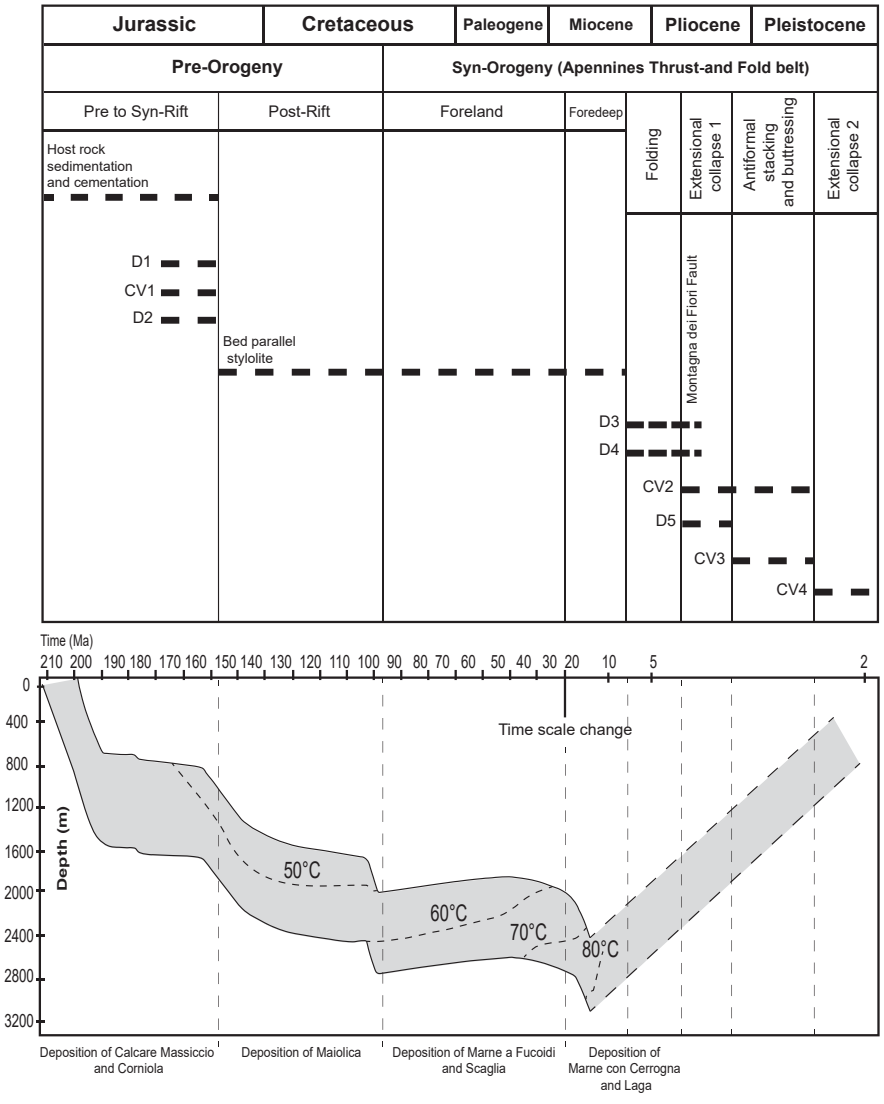


Fig. 14

Solid Earth Discuss., https://doi.org/10.5194/se-2018-136
Manuscript under review for journal Solid Earth
Discussion started: 3 January 2019
© Author(s) 2019. CC BY 4.0 License.

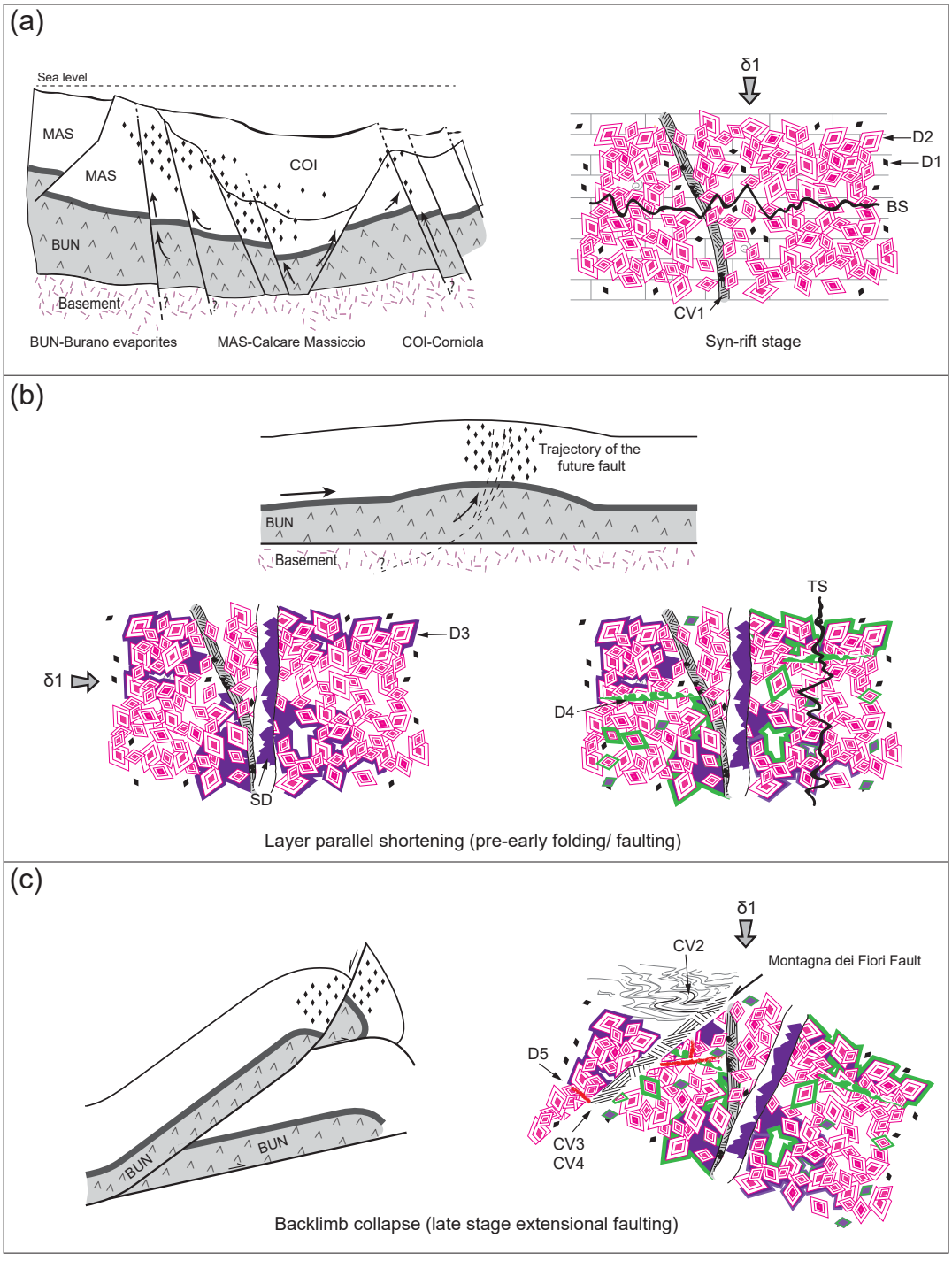


Fig. 15